THREE-DIMENSIONAL NUMERICAL SIMULATION OF PAVEMENTS DEFLECTION BASINS UNDER MOVING LOADS

A Thesis

by

YONG DENG

Submitted to the Office of Graduate and Professional Studies of
Texas A&M University
in partial fulfillment of the requirements for the degree of

MASTER OF SCIENCE

Chair of Committee,	Robert L. Lytton
Co-Chair of Committee,	Luciana R. Barroso
Committee Members,	Anastasia Muliana
	Xue Luo
Head of Department,	Robin Autenrieth

August 2017

Major Subject: Civil Engineering

ABSTRACT

With the development of techniques and increasing need for the evaluation and prediction of pavements' conditions during and after construction, the methodology of nondestructive testing (NDT) is generally applied in the field and on the process of research. This text serves as a review of strengths and limitations of technology and devices used in NDT testing, providing a potential indicator for evaluation and advanced warning, and discussing effects of velocities of testing devices on the responses of pavements. The thesis provide parts of theoretical backgrounds for testing and backcalculation techniques of an improved NDT testing.

CONTRIBUTORS AND FUNDING SOURCES

Contributors

Part 1, faculty committee recognition

This work was supervised by a thesis committee consisting of Professor Robert L. Lytton and Dr. Luciana R. Barroso of the Department of Civil Engineering, Professor Anastasia Muliana of the Department of Mechanical Engineering and Dr. Xue Luo of Texas A&M Transportation Institute (TTI).

Part 2, student/advisor contributions

All work for the thesis proposal was completed by the student, under the advisement of the thesis committee.

Funding Sources

This work was made possible in part by Texas Department of Transportation (TxDOT) under Project Number 0-6869.

Its contents are solely the responsibility of the authors and do not necessarily represent the official views of the Texas Department of Transportation.

NOMENCLATURE

TTI	Texas A&M Transportation Institute
TxDOT	Texas Department of Transportation
NDT	Nondestructive Testing
FWD	Falling Weight Deflectometer
RWD	Rolling Wheel Deflectometer
RDD	Rolling Dynamic Deflectometer

TABLE OF CONTENTS

Page

ABSTRACT ii

CONTRIBUTORS AND FUNDING SOURCES iii

NOMENCLATURE iv

TABLE OF CONTENTS v

LIST OF FIGURES vii

LIST OF TABLES x

1. INTRODUCTION 1

1.1 Introduction to Nondestructive Testing 1
1.2 Typical Equipment and Characteristics 2
1.3 Objectives and Main Tasks 5

2. THEORY 8

2.1 Current Nondestructive Evaluation of Pavement 8
2.2 Properties of Viscoelastic Materials 12
2.3 Theory of Deflection Basin – Pavement Material Property Measuring System 17
2.4 Elastic Solution of Pavement Deflection 20

2.4.1 Analysis of Beams on Elastic Foundation 20
2.4.2 Modification of Modulus of the Foundation 26

2.5 Viscoelastic Solution of Pavement Deflection 29

2.5.1 Laplace Transform of Material Coefficients 29

3. BACKCALCULATION ANALYSIS 32

3.1 Shape of Deflection Basin – Deflection and Slope 32
3.2 Coefficients Backcalculation Using Correspondence Principle 34

4. SIMULATION RESULTS 36

4.1 Construction of Finite Element Models 36
4.2 Material Properties 38
4.3 Results of Simulation 41

4.3.1 Results of 'Visco' Analysis 41
4.3.2 Results of 'Dynamic' Analysis 44

5. SUMMARY AND CONCLUSIONS 49

5.1 Capabilities of New Concept 49
5.2 Future Work 50

REFERENCES 51

APPENDIX A 53

APPENDIX B 57

APPENDIX C 62

LIST OF FIGURES

Page

Figure 1 Force-Time Relationship of FWD Load 8

Figure 2 Deflection-Time Relationship of the Pavement 9

Figure 3 A Moving FWD, Deflection Basin and Complex Modulus 10

Figure 4 Sketch of Travelling Equipment for Deflection Measurement 17

Figure 5 Concept of Characteristic Length of Pavement 18

Figure 6 Illustration of Asymmetric Deflection Basin under a Moving Load..... 19

Figure 7 Beam on Elastic Foundation 21

Figure 8 Vertical Equilibrium State of an Element of the Beam 22

Figure 9 Three Cases of the Beam under Uniform Loads 25

Figure 10 Fitting Curve Using MATLAB 33

Figure 11 Data Comparison 34

Figure 12 Simulation of Moving Load 37

Figure 13 Numerical Model after Meshing 38

Figure 14 Fitted Power-Law Function with Prony - Series Data of Surface (Type 2) 39

Figure 15 Pavement Type 1 under Different Moving Loads Using 'Visco' Analysis 41

Figure 16 Pavements under Moving Loads v= 50mph Using 'Visco' Analysis 43

Figure 17 Pavement Type 1 under Different Moving Loads Using 'Dynamic' Analysis 44

Figure 18 Pavements under Moving Loads v= 50mph Using 'Dynamic'

Analysis 46

Figure 19 Pavement Type 1 under Moving Loads v=50 mph with/without Inertia Damping 47

Figure 20 Pavement Type 1 under Moving Loads v=15 mph with/without Inertia Damping 48

Figure A.1 Fitted Power-law Function with Prony-Series Data of Surface (Type 3) 53

Figure A.2 Fitted Power-law Function with Prony-Series Data of Surface (Type 1) 54

Figure A.3 Fitted Power-law Function with Prony-Series Data of Base (Type 1) ... 54

Figure A.4 Fitted Power-law Function with Prony-Series Data of Base (Type 2) ... 55

Figure A.5 Fitted Power-law Function with Prony-Series Data of Base (Type 3) ... 56

Figure B.1 Pavement Type 2 under Different Moving Loads Using 'Visco' Analysis 57

Figure B.2 Pavement Type 3 under Different Moving Loads Using 'Visco' Analysis 58

Figure B.3 Pavements under Moving Loads v=40 mph Using 'Visco' Analysis 59

Figure B.4 Pavements under Moving Loads v=25 mph Using 'Visco' Analysis 60

Figure B.5 Pavements under Moving Loads v=15 mph Using 'Visco' Analysis 61

Figure C.1 Pavement Type 2 under Different Moving Loads Using 'Dynamic' Analysis 62

Figure C.2 Pavement Type 3 under Different Moving Loads Using 'Dynamic' Analysis 63

Figure C.3 Pavements under Moving Loads v=40 mph Using 'Dynamic' Analysis 64

Figure C.4 Pavements under Moving Loads v=25 mph Using ‘Dynamic’ Analysis 65

Figure C.5 Pavements under Moving Loads v=15 mph Using ‘Dynamic’ Analysis 66

LIST OF TABLES

Page

Table 1 Summary of Nondestructive Testing Devices 3

Table 2 Type of Pavement Responses under a Moving Load 19

Table 3 Sample Data from ABAQUS 33

Table 4 Data Comparison 33

Table 5 Coefficients of Three Flexible Pavements 39

Table 6 Prony Series and Instantaneous Modulus of Surface (Type 2) 39

Table 7 Basic Properties of Surface 40

Table 8 Basic Properties of Base 40

Table A.1 Prony Series and Instantaneous Modulus of Surface (Type 3) 53

Table A.2 Prony Series and Instantaneous Modulus of Surface (Type 1) 53

Table A.3 Prony Series and Instantaneous Modulus of Base (Type 1) 54

Table A.4 Prony Series and Instantaneous Modulus of Base (Type 2) 55

Table A.5 Prony Series and Instantaneous Modulus of Base (Type 3) 55

1. INTRODUCTION*

1.1 Introduction to Nondestructive Testing

The evaluation of pavements' conditions during and after construction is a long-term and essential process for pavements' rehabilitations, corrections and future designs. The methodology of nondestructive testing (NDT) is generally used for its characteristics of reflecting in-situ responses and material properties of pavements as well as not causing any damage to structures. For quantitative or qualitative evaluation, outputs from testing can be divided into two major types - deflections and material properties. The first type is the most straightforward structural response of pavements under loads. Nowadays testing devices are able to collect deflection information such as continuous deflected profiles, maximal or mean values of deflections over testing sections. And the other type of outputs covers dynamic modulus and phase angles which stand for properties of surfaces and supporting layers. Such values can be obtained from mastercurves of deflection-time histories of pavements under dynamic loads using backcalculation procedures.

In order to obtain these two types of outputs, various testing devices are being developed. Based on types of outputs, the nondestructive testing can be divided into the deflection-based and the seismic-based (James et al. 1998). Typical nondestructive testing devices are the falling weight deflectometer (FWD), rolling dynamic deflectometer (RDD), the Applied Research associates' rolling wheel deflectometer (RWD), airfield rolling wheel deflectometer (ARWD), road deflection tester (RDT), and high speed

*Reprinted with permission from Carlson, Paul, et al. *Advancing Innovative High-Speed Remote-Sensing Highway Infrastructure Assessment Using Emerging Technologies*. No. FHWA/TX-16/0-6869-1. 2017.

deflectograph (HSD) which are applied in the field or are in the process of research and development.

1.2 Typical Equipment and Characteristics

Falling Weight Deflectometer (FWD) is one of the most widely used nondestructive testing devices so far. It is able to generate haversine-shaped dynamic loads of which the duration and peak values can be adjusted by different mass, stiffness and dropping height of the circular loading cell. The time history of deflections can then be measured by the sensors mounted along the centerline of the load plate. For each testing location, technicians must stop the test vehicle to perform the FWD deflection measurements which will require traffic control. The deflections obtained from the FWD are non-continuous.

The RDD is a nondestructive testing device designed and developed at the University of Texas at Austin which consists of a vibroseis truck and a servo-hydraulic vibrator to generate dynamic load. The dynamic forces are transferred to the pavement and the vertical deformations are measured by four rolling deflection sensors. The RDD can provide a continuous moving deflection basin profile of pavements with sufficient accuracy, but the operational velocity is 1 mph for the first generation and up to 3 mph for the second generation (Lee and Stokoe, 2006), which means interruption is also caused to the traffic.

The RDD loading system can also be used with other geophysical devices such as Ground Penetrating Radar (GPR) in the Total Pavement Acceptance Device (TPAD). The operational speed can reach up to 10 mph with much greater rolling noises to loading and

data acquisition systems (Stokoe et al. 2013). The RWD is a deflection-based device which is designed and manufactured by the Applied Research Associates (ARA). It is constructed using a specially designed 53-ft long tractor-trailer to apply a load of 18,000 lb to the pavement and measures the single moving deflection responses using high precision laser distance measuring devices. Deflection is the vertical difference between the deflected and un-deflected profiles. The RWD can run at a highway speed (e.g., 55 mph), but it produces relatively high variance and limited accuracy of deflection, which can be used to qualitatively evaluate the pavement structural capacity but not quantitatively.

Comparisons of these three devices have been conducted and are summarized in Table 1.

Nondestructive Testing Devices	Operational Speed	Type of Applied Force	Type of Measured Data
RDD	1 to 3 mph	Dead Weight on Wheels + Dynamic Loads on Loading Cells	Continuous
RWD	45 to 65 mph	Dead Weight on Wheels	Continuous
FWD	0	Dynamic Loads on Loading Cells	Discrete

Table 1. Summary of Nondestructive Testing Devices

Nondestructive Testing Devices	Daily Production	Deflection Sensor Accuracy	Distance between Readings
RDD	9 miles	0.05 mils	2 to 3 ft
RWD	36 miles	± 2.75 mils	0.5 in
FWD	100-300 locations	N/A	12 in

Note: 1 mil = 0.001 inches

Table 1 Continued

The information obtained from NDT devices are based mainly upon the type of loads applied to pavements and data acquisition systems. First, it is generally acknowledged that there is a tradeoff between operational speeds of testing vehicles and the precision of the data. Deflections obtained from RWD and RDD are often required to be compared with FWD results to prove their accuracy, repeatability and sensitivity. Besides, in spite of the interval between adjacent measured data, deflections over a unit length (e.g., 100 feet for RWD) are averaged for qualitative evaluations. Second, mastercurves of deflection-time histories of pavements under dynamic loads generated by FWD can be used for backcalculation of dynamic properties such as dynamic modulus and compliance. This cannot be done with the measurements made by the RDD and RWD which are the maximum deflections. With continuous measurement, the largest deflections can only be used to indicate the weakest pavement sections.

The FWD, as the most commonly used nondestructive device, can effectively measure the deflection data of the pavement under dynamic loads as well as provide deflection-time histories for the stiffness and other dynamic properties of the pavement. However, it has obvious weakness – the user time delay due to the 'stop-and-go' testing procedure of the FWD. The time delay will significantly increase costs for the traffic control and induce safety problems to technicians. Meanwhile, the low productivity of the testing makes it difficult to obtain real-time conditions of the pavement and make the best decisions on the timing of pavement maintenance so as to expect the longest service life and the least maintenance costs.

1.3 Objectives and Main Tasks

The objective of this thesis is to develop a series of numerical pavement models with material properties reflecting deteriorating pavement conditions under increasing load cycles. Then obtain and compare deflection basins of these pavements under moving loads with different speeds. The results will provide potential analytical support for developing NDT techniques with highway-speed operations which produce the rate of change of the modulus and phase angle of the asphalt surface layer to provide an advance warning of pavements' failure.

The potential benefits of the technology advancement are:

- The highway-speed deflection measuring system will produce a continuous deflection profile for a pavement to replace the existing deflection test at random locations such as the falling weight deflectometer (FWD).
- The highway-speed deflection measuring system will eliminate the potential user

time delay costs and avoid safety problems resulting from the traffic control required by the traditional deflection test. The moving deflection measuring system can be operated at normal highway speed, e.g., 60 mph, thus it will cause no disruptions to the traffic.

- The pavement manager can employ this system to obtain real-time conditions of the pavement and make the best decisions on the timing of pavement maintenance so as to expect the longest service life, the least maintenance costs and the least delay costs.
- The pavement construction engineers can use this system to locate, fix, and eliminate the weak spots of pavement structures at the time of construction, and eventually to assure quality construction to reduce life cycle costs and expect a longer service life.
- Advance warning of developing pavement distress to permit rational pavement maintenance and rehabilitation managements.

Due to the aspects of moving speed increase and the deflection data measurement technology improved in the task, the primary work finished are:

- Develop methodology for fitting the deflection basins under loads of highway speed and back calculating pavement layer properties with the deflection data measured by the equipment.
- Develop numerical models with finite element software to explore the characteristics of deflection basins under various moving speed and layer properties.

- Compare theoretical methodology and numerical models, discuss the potentiality of the methodology.

2. THEORY*

2.1 Current Nondestructive Evaluation of Pavement

As described in the previous section, the Falling Weight Deflectometer (FWD) is a typical nondestructive pavement evaluation device. It can produce transit impulse loading by the loading plate. The resulting deflections of points at given distances from the plate can be collected by geophones and the deflection basin of the pavement can be determined.

As a device applying loads different from RDD and RWD, the FWD sets dynamic loads of which two peaks simulate vehicles with two axles and then records time histories of responses of the pavement through sensors, as illustrated in Figure 1 and Figure 2. Because of these characteristics, the deflection basin measured by the FWD can be treated as the actual deflection basin of the pavement under moving loads.

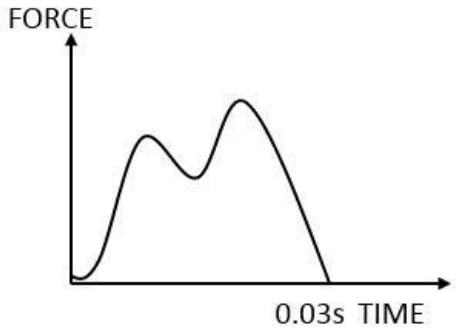

Figure 1. Force-Time Relationship of FWD Load

*Reprinted with permission from Carlson, Paul, et al. *Advancing Innovative High-Speed Remote-Sensing Highway Infrastructure Assessment Using Emerging Technologies*. No. FHWA/TX-16/0-6869-1. 2017.

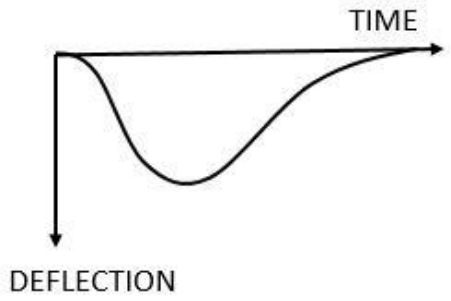

Figure 2. Deflection-Time Relationship of the Pavement

For most backcalculation cases, the peak load and deflection are extracted from graphs of load versus time impulses and deflection versus time response created by the FWD to evaluate elastic material properties. However, there is much more information in these signals. Lytton pointed out that as the falling weight drops to the pavement surface, the impulse load creates surface waves and body waves which move in the pavement (Lytton 1989). If a fast Fourier transform is performed on the impulse and response, signals will be transformed into forms of frequency-dependent components which are complex numbers for each frequency. The modulus of different materials of layers can be represented as this kind of complex modulus (Lytton 1989).

$$E^*(f) = E'(f) + iE''(f) \quad (1)$$

where,

$E^*(f)$ – the complex modulus

$E'(f)$ – the real part of the complex modulus, which is the in-phase component of stress divided by the strain

$E''(f)$ – the imaginary part of the complex modulus which is made up of the lagging component of the stress divided by the strain.

It is believed that there exists a time lag between the response of the pavement and the impulsive load. Figure 3 shows a lag distance between locations where the load acts and the maximal deflection occurs. The time lag can be explained and represented by the phase angle of the system which consists of two parts: the time lag due to the propagation of waves in the pavement and the material damping. There is a relationship between the lag angle ϕ and material damping ratio β.

$$2\beta = \tan\phi(f) = \frac{E''(f)}{E'(f)} \tag{2}$$

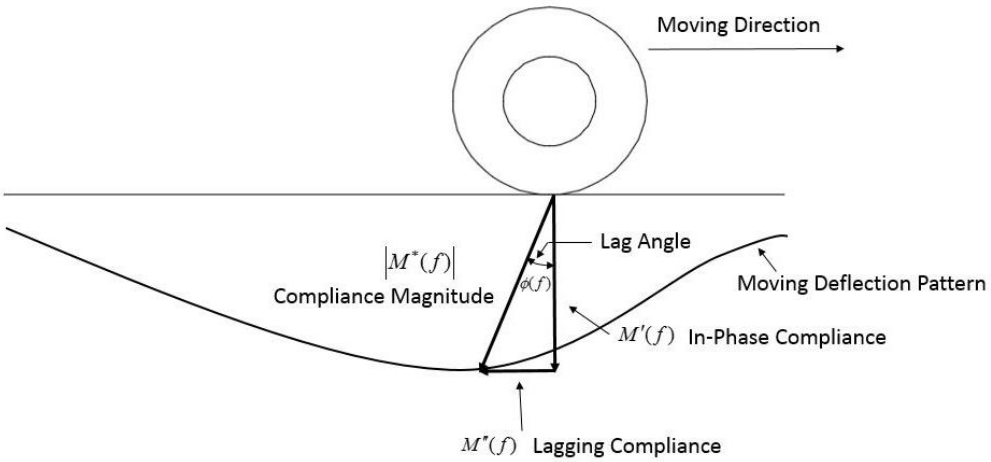

Figure 3. A Moving FWD, Deflection Basin and Complex Modulus

From the left part of Equation (2), it can be observed that the value of the lag angle relies merely on the damping ratio of the material which is independent of the properties of external loads. However, from the other part, there is an obvious relationship between the lag angle and the ratio of the real part and the imaginary part of the complex modulus, both of which are frequency-dependent.

The concept of phase angle effectively explains the time lag between the response of the pavement and the impulsive load which is commonly shown in time histories of

loads and deflections in FWD testing. Also, it combines the material damping which is a typical property of inelastic material with dynamic properties. Hence, from measured data in FWD testing, more information can be obtained to reflect and evaluate actual properties of pavement layer materials and structures.

In modern transportation, high speeds, heavy loads and great capacities of vehicles are three important factors which should be considered in designs and evaluations of pavements (Sun and Deng 1998). Speeds of vehicles, especially highway speeds, should be introduced to insitu and laboratory testing for both improving the effectiveness and representing traffic conditions in reality.

Many researches have been conducted for evaluating effects of loads, pavements and their interaction on responses of pavements in order to obtain simplified models including necessary factors. Specifically, the importance of speed and frequency of vehicles in responses of flexible pavements has been discussed separately (Hardy and Cebon 1991). In a dynamic pavement response model, strain magnitudes of base and soil decrease and move further behind the load when vehicle speed increases. This idealized dynamic response model (Cebon 1988) focuses on the dynamic properties of vehicles and pavements which can be simplified as combinations of springs and dampers. Results of this research have shown contributions of the velocity to the responses of pavements which include the lag behind loads and the magnitude. It can be concluded that from the viewpoint of dynamics, the whole system is sensitive to the velocities of vehicles.

In flexible pavements, both surfaces and base courses are inelastic materials. The dynamic behavior of inelastic materials especially viscoelastic materials have been studied

and analytical methods have been developed. The term ‘dynamic’ used in some experiments and contexts has no connection with structural dynamics such as inertial damping or resonance. Instead, the viscosity of materials is focused to describe the response to loads with different frequencies. For example, in a viscoelastic material under a sinusoidal load with cycle ‘T’, time histories of stress and strain are sinusoids out of phase (Lakes 2009). The phase shift can be expressed as

$$\delta = \frac{2\pi \bullet \Delta t}{T} \tag{3}$$

where Δt is the lag time between stress and strain and δ is the phase angle of the viscoelastic properties.

2.2 Properties of Viscoelastic Materials

For elastic solids, the stress is proportional to the strain. The strain of the object will not change when the stress is fixed at a constant value. The ratio of the stress and strain is the Young’s modulus E. For a viscous fluid, the force applied is proportional to the rate of elongation. The ratio is denoted as the viscosity. For a linear viscous material, if the strain is held constant from the beginning, the stress will increase to the required value then decrease to zero with time. Different from these materials of which strain (force) is ideally proportional to strain or its time derivative, viscoelastic materials are those for which the relationship between stress and strain depends on time. The properties of viscoelastic materials can be described by creep and relaxation.

Creep is a progressive deformation of a material under constant stress.

$$J(t) = \frac{\varepsilon(t)}{\sigma_0} \tag{4}$$

where,

J – creep compliance

ε – strain of the material

σ – stress of the material

For a viscoelastic material, it is typically that the strain increases with fixed stress and decreases toward zero when the stress vanishes. The creep compliance of a viscoelastic solid will eventually increase to a boundary value, while for a viscoelastic fluid, it will increase to infinity.

Relaxation is a progressive decrease of stress when the strain remains constant.

$$E(t) = \frac{\sigma(t)}{\varepsilon_0} \tag{5}$$

where,

E – relaxation modulus

ε – strain of the material

σ – stress of the material

E represents the stiffness of the material which is the Young's modulus in elastic materials. For viscoelastic materials, the relaxation modulus is a function of time and decreases with a fixed strain. The relaxation modulus of a viscoelastic solid has a limit value greater than zero when time approaches infinity.

Asphalt is a typical material for the surface of pavements and shows characteristics of viscoelastic solids. For convenience of prediction and analysis of material properties,

series of exponentials, power laws, and logarithmic functions are used to represent creep compliance and relaxation modulus varying with time (Lakes 2009).

In this thesis, the Power Law and Prony-series models are applied to represent the creep and relaxation function. The Power Law equation

$$E(t) = E_1 t^{-m} \tag{6}$$

is mainly used in the backcalculation of material property coefficients for its simplicity but including key variables which sufficiently represent modulus of viscoelastic solids varying with time. In the programming of backcalculation, small number of coefficients contributes to relatively simpler calculation. Physical meaning of m will be introduced later and deflection basins will be compared with different values of m to describe the importance to backcalculate it.

The coefficients of Prony-series can be defined directly by users in the commercial finite element software (ABAQUS 2010). By defining instantaneous elastic modulus E_0 and certain sets of shear modulus ratios g_i, bulk modulus ratios k_i and relaxation times τ_i, based on the relationship between shear, bulk and elastic modulus, time-dependent shear, bulk and elastic modulus can be determined.

$$G(t) = G_0 \left[1 - \sum_{i=1}^{n} G_i \left(1 - e^{-t/\tau_i} \right) \right] \tag{7}$$

$$K(t) = K_0 \left[1 - \sum_{i=1}^{n} K_i \left(1 - e^{-t/\tau_i} \right) \right] \tag{8}$$

where $G(t)$ and $K(t)$ are relaxation shear and bulk modulus, G_0 and K_0 are instantaneous shear and bulk modulus which can be transferred from user-defined

instantaneous elastic modulus E_0. Based on the relationship between shear, bulk and elastic modulus as well as other input coefficients, the relaxation modulus of a linearly viscoelastic material can be expressed as

$$E(t) = E_\infty^a + \sum_{i=1}^{n}\left(E_i^a e^{-\frac{t}{\tau_i}}\right) \tag{9}$$

where E_∞^a, E_i^a and τ_i are regression coefficients in the model and satisfy the equations below.

$$E_i^a = E_i E_0 \tag{10}$$

$$E_\infty^a = E_0 - \sum_{i=1}^{n} E_i^a \tag{11}$$

$$E_i = g_i = k_i \tag{12}$$

The dynamic modulus is given by

$$E'(\omega) = E_\infty^a + \sum_{i=1}^{n}\frac{\omega^2\tau_i^{\,2}E_\infty^a}{1+\omega^2\tau_i^{\,2}} \tag{13}$$

$$E''(\omega) = \sum_{i=1}^{n}\frac{\omega\tau_i E_\infty^a}{1+\omega^2\tau_i^{\,2}} \tag{14}$$

$$\left|E^*\right| = \sqrt{E'^2 + E''^2} \tag{15}$$

$$\tan\phi = \frac{E''}{E'} \tag{16}$$

where $E'(\omega)$ and $E''(\omega)$ are the storage and loss modulus respectively, ω is the angular velocity, $\left|E^*\right|$ is the magnitude of the dynamic modulus, ϕ is the phase angle. From Equation (13) ~ (16), it can be seen that the magnitude and phase angle of modulus depend

upon the frequencies of loads. As mentioned before, in current FWD tests, the transient deflection of the pavement is measured after impulsive loads are applied. The peak load and peak deflection are assumed to be static measurements and elastic parameters are back-calculated. Actually, parameters representing the viscoelasticity of materials can play a similar or better role. Experiments have been conducted to show that as an asphalt mixture cracks under repeated loading, the dynamic modulus decreases slowly as the phase angle increases almost linearly (Reese, 1997).

After construction, an asphalt surface layer has the maximal value of modulus and low phase angle. With repeated loading, the modulus decreases due to fatigue and fractures while the phase angle is increasingly greater. An approximate relationship (Lytton 1989) between phase angle and the value of m as in Equation (6) is

$$\phi = \frac{\pi}{2} m \tag{17}$$

In Reese's work, the phase angle approaches its maximal value around 34 degrees, when the pavement is about to fail. After that, the pavement develops large cracks completely through the surface layer. Hence, if the modulus and phase angle (or m) can be measured during the service of a pavement, the current and impending conditions of the pavement can be effectively evaluated and predicted.

2.3 Theory of Deflection Basin – Pavement Material Property Measuring System

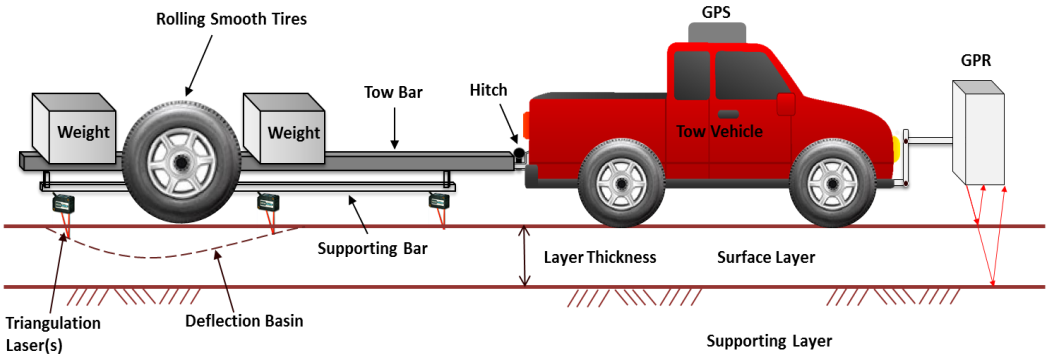

Figure 4. Sketch of Travelling Equipment for Deflection Measurement

Figure 4 illustrates a potential testing equipment for measuring deflection under moving loads. Eventually, this apparatus will measure the moving deflection basin at highway speeds under pavement design loads, and determine analytically the viscoelastic material properties of the surface layer and the supporting layers of both concrete and asphalt pavements. Previous measurements made on Texas pavements have indicated that the characteristic length of such pavements is approximately 20–30 ft. The characteristic length is defined as the decorrelation distance of a pavement in which the surface roughness pattern at one point is decorrelated from the roughness pattern at a second point one decorrelation distance away. Figure 5 shows typical Texas pavement decorrelation distances.

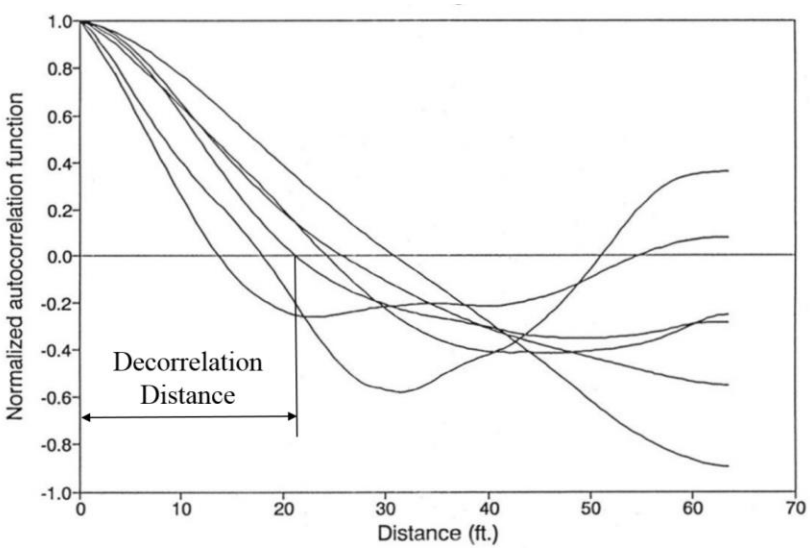

Figure 5. Concept of Characteristic Length of Pavement

Within the distance, pavements will respond to moving loads and the effects of viscoelasticity of the materials will appear in the shapes and magnitudes of the deflection basins.

Concrete pavements are expected to respond to the moving loads as an elastic surface layer with a viscoelastic supporting layer, the softness of which is indicative of expected rapid deterioration of the concrete pavement distress. Asphalt pavements are expected to respond to the moving loads as viscoelastic layers in both the surface and supporting layers. Aged and brittle asphalt will respond as being more elastic until cracks begin to appear, either growing from the bottom up or from the top down. As such, these measurements will be an advance indicator of future pavement cracking. The softer supporting layers will, as with the concrete pavements, indicate a more rapid deterioration rate of cracking and of rutting. Stabilized supporting layers will respond as being more elastic until cracks begin to appear, reducing the effective support they provide to the

surface layer. Water entering these supporting layers will soften them, making them respond in a more viscoelastic way. Table 2 shows these four pavement responses.

Pavement Type	Type of Pavement Responses	
	Surface Layer	Supporting Layer
Asphalt	Viscoelastic	Viscoelastic
Concrete	Elastic	Viscoelastic
Asphalt over Stiffness Support	Viscoelastic	Elastic
Concrete over Stiffness Support	Elastic	Elastic

Table 2. Type of Pavement Responses under a Moving Load

Viscoelastic responses will produce an asymmetric deflection basin with a steep leading edge and a shallow trailing edge, as shown in Figure 6. The greater the maximum deflection and steeper the leading edge indicate pavements that are more susceptible to load-related distress.

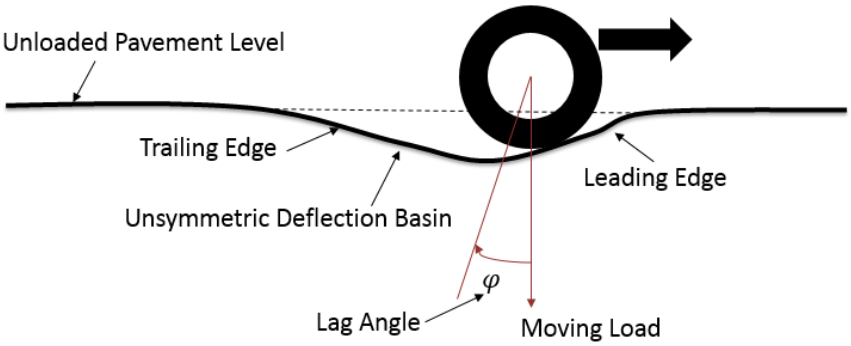

Figure 6. Illustration of Asymmetric Deflection Basin under a Moving Load

Having such information acquired at highway speeds for every characteristic length of the pavement along its entire length will pinpoint trouble spots long before serious distress begins to develop. This makes possible an effective planning program for maintenance and rehabilitation of entire pavement networks.

This thesis is to study characteristics of the actual deflection basin, figure out factors affecting it and then provide a potential backcalculation method for those important material property coefficients. From the data collected from the geophone. It is clear that the whole deflection basin shows obvious asymmetry. It is likely that the inelasticity of the pavement and foundation cause such a phenomenon. Hence, in this thesis, the supporting layer (base course) will be processed as a viscoelastic material. Improved expressions and parameters will be applied as those of surface layer to reflect the real situation better.

2.4 Elastic Solution of Pavement Deflection

2.4.1 Analysis of Beams on Elastic Foundation

The solution of beams on elastic foundation (Hetenyi 1946) calculates the deflection of an arbitrary point along a pavement under various types of loading. A beam-on-elastic foundation solution can be applied in the back calculation of material properties of both the surface and supporting layer with measured deflection data. The assumption made in the beam-on-elastic foundation solution is that the beam is supported on an elastic foundation. A unit deflection of the beam will cause relevant reaction of the foundation as illustrated in Figure 7. The assumption and calculation method for the reaction of the foundation was introduced by Winkler in 1867.

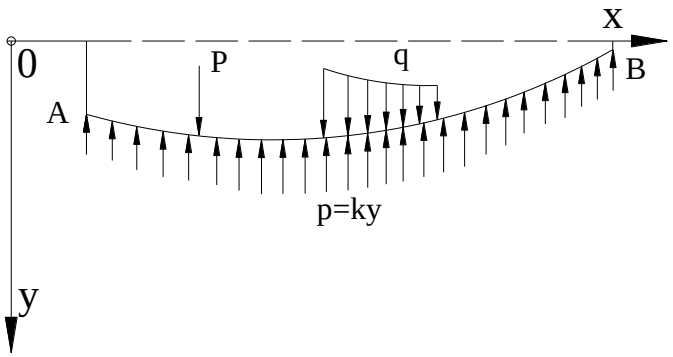

Figure 7. Beam on Elastic Foundation

Assume that a beam is supported on the foundation and acted upon by a concentrated load, the equation of external force acting on the beam can be expressed as:

$$p = bk_0 y = ky \tag{18}$$

p – reaction load of the foundation per unit length

b – width of the beam

y – deflection of the beam

k_0 – modulus of the foundation

The form of the reaction follows Hooke's law and the value is proportional to all three dimensions. Having defined the reaction of the foundation, based on the equilibrium state of the beam (Figure 8), the summation in the vertical direction can be expressed as,

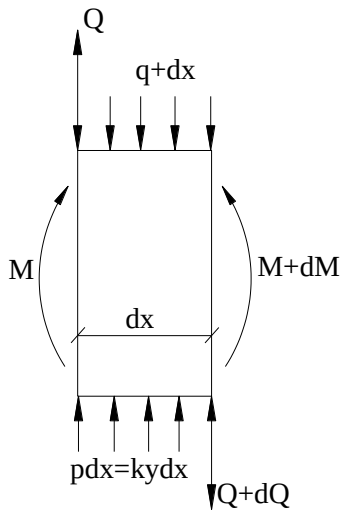

Figure 8. Vertical Equilibrium State of an Element of the Beam

$$Q-(Q+dQ)+kydx-qdx=0 \tag{19}$$

It can be simplified that,

$$\frac{dQ}{dx}=ky-q \tag{20}$$

Based on the known conditions that the shear force is the first derivative of the moment,

$$Q=\frac{dM}{dx} \tag{21}$$

and the differential equation of a beam in bending,

$$EI\frac{d^2y}{dx^2}=-M \tag{22}$$

$E-$ elastic modulus of the beam

$I-$ moment of inertia of the cross section of the beam

by using Equation (19)~(22), it can be derived that,

$$EI\frac{d^4y}{dx^4}=-ky+q \tag{23}$$

The solution of the differential Equation (23) can be obtained from the homogeneous part and a particular part corresponding to q. Especially when the beam is loaded by an individual concentrated load, the solution will consist of the homogenous part only.

For the homogeneous part, assume that

$$y = e^{mx} \tag{24}$$

Then, substitute Equation (24) into (23), four roots of two different values can be obtained.

$$m_{1,2,3,4} = \sqrt[4]{\frac{k}{4EI}}(\pm 1 + i) \tag{25}$$

in which the factor $\sqrt[4]{\frac{k}{4EI}}$ is called the characteristic of the system, denoted as λ, the dimension is length^{-1}.

So, the solution of the homogeneous part is

$$y = A_1 e^{\lambda(1+i)x} + A_2 e^{-\lambda(1+i)x} + A_3 e^{\lambda(-1+i)x} + A_4 e^{-\lambda(-1+i)x} \tag{26}$$

Replace the complex index with the trigonometric functions,

$$\begin{cases} e^{i\lambda x} = \cos\lambda x + i\sin\lambda x \\ e^{-i\lambda x} = \cos\lambda x - i\sin\lambda x \end{cases} \tag{27}$$

Equation (26) can be expressed as

$$\begin{aligned} y = {} & e^{\lambda x}\left[\cos\lambda x(A_1 + A_4) + \sin\lambda x(A_1 i - A_4 i)\right] \\ & + e^{-\lambda x}\left[\cos\lambda x(A_2 + A_3) + \sin\lambda x(A_2 i - A_3 i)\right] \end{aligned} \tag{28}$$

Assume that,

$$\begin{cases} A_1 + A_4 = C_1 \\ i\left(A_1 - A_4\right) = C_2 \\ A_2 + A_3 = C_3 \\ i\left(A_3 - A_2\right) = C_4 \end{cases} \tag{29}$$

The solution can be rewritten as follows,

$$y = e^{\lambda x}\left(C_1 \cos \lambda x + C_2 \sin \lambda x\right) + e^{-\lambda x}\left(C_3 \cos \lambda x + C_4 \sin \lambda x\right) \tag{30}$$

In order to obtain the four parameters $C_1 \sim C_4$ of the Equation (30), actual boundary conditions should be taken into consideration. First, compared to the length of the pavement, no matter what the loading form is, the wheel of vehicles or loading plates, the scale of the loading along the pavement is fairly small. Hence, it is reasonably assumed that, at the spot long enough from the loading area, the deflection approaches zero. The terms including $e^{\lambda x}$ vanish in the Equation (30), which becomes

$$y = e^{-\lambda x}\left(C_3 \cos \lambda x + C_4 \sin \lambda x\right) \tag{31}$$

Second, when the beam is acted on by a concentrated load, the deflection would show a characteristic of symmetry from two sides of the loading point, which means that the first derivative of Equation (31) would be zero at the point $x = 0$.

$$y'\big|_{x=0} = e^{-\lambda x}\left[\left(C_4 - C_3\right)\lambda \cos \lambda x - \left(C_4 + C_3\right)\lambda \sin \lambda x\right] = 0 \tag{32}$$

So, it can be derived that,

$$C_4 = C_3 = C \tag{33}$$

Then, back to the equilibrium state of the beam, the beam is acted on by the concentrated force and reaction from the foundation, which should counteract in the equilibrium state of the beam.

$$P = 2\int_0^\infty kydx = 2kC\int_0^\infty e^{-\lambda x}\left(\cos\lambda x + \sin\lambda x\right)dx \tag{34}$$

Eventually,

$$C = \frac{P\lambda}{2k} \tag{35}$$

Therefore, the deflection of a beam of unlimited length acted by a concentrated load can be expressed as

$$y = \frac{P\lambda}{2k}e^{-\lambda x}\left(\cos\lambda x + \sin\lambda x\right) \tag{36}$$

When the beam is under uniform loads, the analysis procedures are similar. The uniform load can be treated as a combination of multiple concentrated loads, therefore, the deflection can be calculated by the integral of multiple deflections under concentrated loads. As the location of the calculated point varies, the deflection can be divided into three types when the beam is under uniform load.

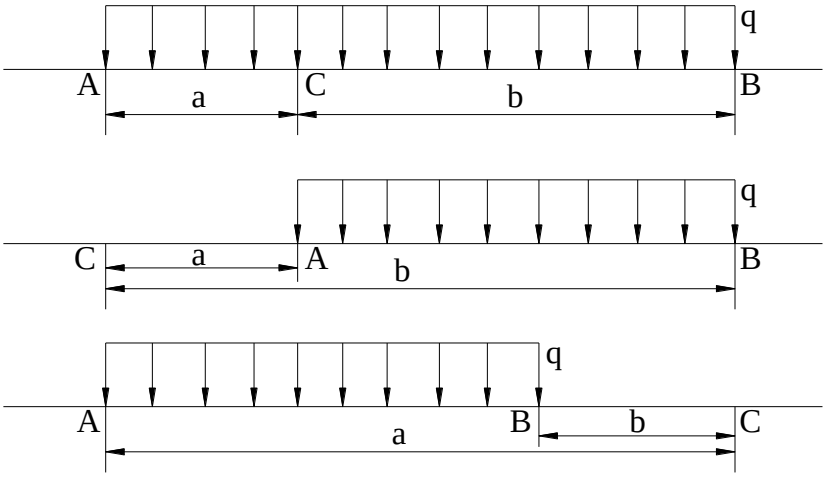

Figure 9. Three Cases of the Beam under Uniform Loads

Figure 9 shows that the point needs calculating is located under and at two sides of the loading, the deflection of point C can be expressed separately as

$$\begin{cases} y_1 = \dfrac{q}{2k}\left(2 - e^{-\lambda a}\cos\lambda a - e^{-\lambda b}\cos\lambda b\right) \\ y_2 = -\dfrac{q}{2k}\left(e^{-\lambda a}\cos\lambda a - e^{-\lambda b}\cos\lambda b\right) \\ y_3 = \dfrac{q}{2k}\left(e^{-\lambda a}\cos\lambda a - e^{-\lambda b}\cos\lambda b\right) \end{cases} \tag{37}$$

Though Hetenyi's solution expresses sensible assumptions, analysis and calculation methodd for the deflection of the beam under various types of loading, the parameters applied in this method are not time-dependent thus none of them are representative when the loading in this task is at highway speed. The form of the deflection equation, the parameters of the beam and foundation should be modified to represent their dynamic characteristics.

2.4.2 Modification of Modulus of the Foundation

As for soil-structure interaction problems, Winkler's assumption is applied broadly which denotes k_0 as the modulus of foundation and the reactive pressure the foundation acts on the beam is proportional to the vertical deflection of the foundation like an elastic spring (see Equation(18)). Beam-on-elastic foundation solution does not contain any description for the determinant of the modulus k_0. Actually in early research, the modulus k_0 is taken as a known constant for a given type of foundation. The reaction at a given point is related only to the modulus at that point and the whole foundation system is like an individual spring laying at intervals under the beam.

In 1955, Terzaghi pointed out that the reaction of subgrade is correlated to the elastic properties as well as the dimensions of the area acted upon. (Terzaghi 1955). In

1937, Biot published a paper determining the relationship of the modulus k_0 and properties of the soil and the beam (Biot 1937). He pointed out when a concentrated load acted on a three-dimensional subgrade, by evaluating the maximum bending moment the correlation with the Winkler's model for the maximum moment could be expressed as

$$k = \frac{0.95E_s}{(1-\nu_s{}^2)}\left[\frac{E_s B^4}{(1-\nu_s{}^2)EI}\right]^{0.108} \tag{38}$$

where

E_s – elastic modulus of the soil

I – moment of inertia of the beam

ν_s – Poisson's ratio of the soil

E – elastic modulus of the beam

B – width of the beam

Also, in 1961, Vesic extended such situation by considering deflection, shear and moment distribution along the beam (Vesic 1961).

$$k = \frac{0.65E_s}{(1-\nu_s{}^2)}\sqrt[12]{\frac{E_s B^4}{EI}} \tag{39}$$

Above are two examples of relations researchers found about the modulus of the soil and properties of the beam and soil. Later researchers figured out that the modulus of the soil is a complex parameter affected by the distribution of loading, thickness of the surface and many other factors which represent the characteristics of the whole system.

The modulus k_0 will be expressed in a new form in this task. In *Design and Construction of Post-Tensioned Slabs-on-Ground (2nd edition)*, when it comes to

differential deflection distance, for slabs over 50 feet, the effective distance for determining the allowable differential deflection is 6β (β is the characteristic length) rather than the entire length of slabs. Similarly, transform the modulus of the soil from k_0 to E_2 and λ .

$$k = \frac{E_2}{6/\lambda} \tag{40}$$

where

E_2 – elastic modulus of the soil

λ – characteristic of the system (length^{-1})

For convenience, denote $1/\beta$ as the characteristic length.

$$\beta = \lambda = \sqrt[4]{\frac{k}{4EI}} = \sqrt[4]{\frac{E_2}{4E_1 I \bullet 6/\beta}} \tag{41}$$

where,

E_1 – elastic modulus of the beam

E_2 – elastic modulus of the soil

I – moment of inertia of the beam, $I = \frac{bh^3}{12}$, b, h are the width and height of the cross section of the beam respectively

β – characteristic of the system (length^{-1})

From the Equation (41),

$$\beta = \frac{1}{h}\left(\frac{E_2}{2E_1}\right)^{1/3} \tag{42}$$

$$k = \frac{1}{6h}\frac{\left(E_2\right)^{4/3}}{\left(2E_1\right)^{1/3}} \tag{43}$$

In the task, the surface of the pavement can be seen as the 'beam' on the foundation and h is the thickness respectively.

2.5 Viscoelastic Solution of Pavement Deflection

2.5.1 Laplace Transform of Material Coefficients

Beam-on-elastic foundation solution is based on the assumption that both pavement and foundation materials are linear elastic which are independent of time. Such assumption cannot explain the asymmetry of deflection basins. Moreover, viscoelastic properties of surface and viscoelastic properties of supporting layers are of vital importance to evaluating and predicting the current and impending conditions of the pavement. Therefore, in this thesis, material property coefficients are required to be expressed as time or frequency dependent functions and certain coefficients will be backcalculated.

In previous sections, a power-law function and a Prony-series express the modulus of viscoelastic materials as time-dependent functions. Equation (6) ~ (9) express the relationship between relaxation modulus and time which effectively represent the characteristic of viscoelastic solids. As time approaches infinity, the relaxation modulus decreases to a value greater than zero. For the time dependent modulus and frequency dependent modulus, Laplace transform is applied. For Equation (6),

$$E(s) = \mathrm{L}\left[E(t)\right] = \int_0^\infty E_1 t^{-m} e^{-st} dt = E_1 s^{m-1} \Gamma(1-m) \tag{44}$$

where the gamma function Γ is defined as follows

$$\Gamma(m) = \int_0^\infty t^{m-1} e^{-t} dt = (m-1)! \tag{45}$$

The reason why Laplace transform is applied to obtain time-dependent viscoelastic response is that Laplace transformed equations of viscoelastic responses are identical with the responses of an elastic material. Laplace Transformed solutions can be calculated by standard elastic analysis, and then inverted to obtain the time-dependent response (Cost 1964). For the relationship between the time-dependent response of one viscoelastic material and its transformed response, an approximate inverse Laplace transform was developed by Schapery (1975).

$$E(t) \cong \left[sE(s)\right]_{s=\frac{1}{2t}} \tag{46}$$

s is a real and non-negative parameter in Laplace transform. In approximation method, the value evaluated for s is $\frac{1}{2t}$.

No matter what expression (Equation (6) or Equation (9)) is applied to express the time-dependent modulus of viscoelastic surface of the pavement, Laplace transform can provide efficient approximation of time dependent modulus of viscoelastic materials. Similarly, the modulus of the viscoelastic base can also be written in a Power law form as in Equation (6). Hence, coefficients k and β in Equation (42) and (43) can be transformed into time-dependent terms.

$$k(t) = \frac{1}{6h}\frac{\left[E_2(t)\right]^{4/3}}{\left[2E_1(t)\right]^{1/3}}$$
$$k(t) \cong \left[sk(s)\right]_{s=1/2t} \tag{48}$$

$$\beta(t) = \frac{1}{h}\left[\frac{E_2(t)}{2E_1(t)}\right]^{1/3}$$
$$\beta(t) \cong \left[s\beta(s)\right]_{s=1/2t} \tag{49}$$

where $E_1(t), E_2(t)$ are the time-dependent modulus of surface and base respectively.

3 BACKCALCULATION ANALYSIS*

3.1 Shape of Deflection Basin – Deflection and Slope

Figures 3 and 6 show deflection basins of pavement under moving load. From those graphs, distances between the locations where maximal deflection and zero deflection happen are not equal. In order to obtain such asymmetric deflection shape using data measured by lasers set on the tow vehicle, Gumbel probability density curve (Gumbel 1935) is applied in this task.

$$W(x) = W_0 e^{-(\rho/x)^{\beta}} \tag{50}$$

where,

$W(x)$ – the cumulative probability curve of the Gumbel distribution.

x – the measuring distance.

$W_0,\ \rho,\ \beta$ – the model coefficients.

The shape of slope of Gumbel probability density curve is similar to the asymmetric deflection basin. Five measured data by lasers are enough to calculate coefficients $W_0,\ \rho,\ \beta$ which can be applied to obtain an approximation function of the whole deflection basin. For curve fitting, the reference point at which the deflection equals zero is set to be advanced to the vehicle.

Take four sets of data from ABAQUS results and use 'nlinfit' commander in a mathematics software (MATLAB 2015), the model coefficients can be obtained. The results from ABAQUS and fitting results are shown in Table 3 and Figure 10 separately.

*Reprinted with permission from Carlson, Paul, et al. *Advancing Innovative High-Speed Remote-Sensing Highway Infrastructure Assessment Using Emerging Technologies*. No. FHWA/TX-16/0-6869-1. 2017.

From Table 4, it can be seen that Gumbel probability density curve can represent the shape of the deflection basin to some extent.

Distance from Trailing Reference Point (ft)	Deflection (in)
7.779	-1.909E-02
8.779	-2.344E-02
10.779	-1.828E-02
11.779	-1.284E-02

Table 3. Sample Data from ABAQUS

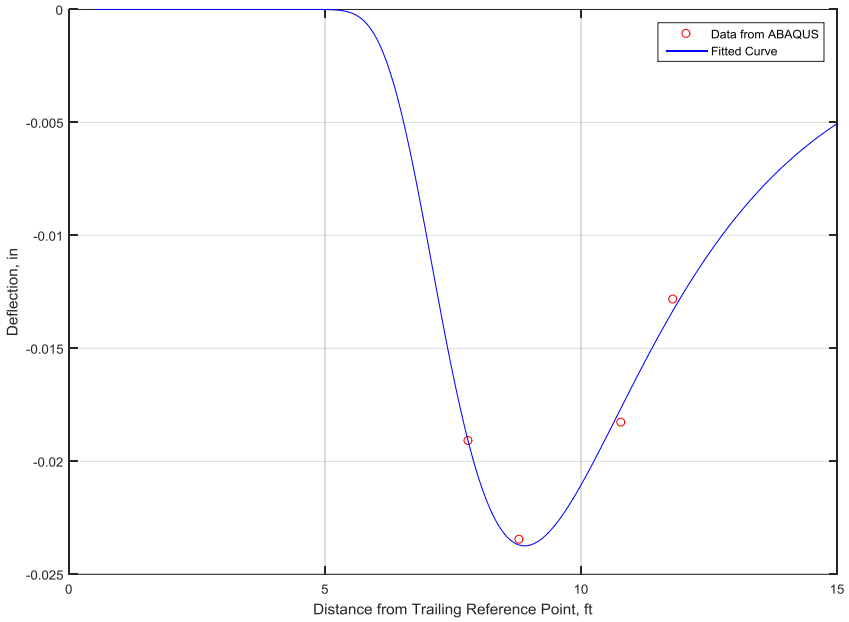

Figure 10. Fitting Curve Using MATLAB

Laser Number	Data from ABAQUS (in)	Data from Fitted Curve (in)	Relative Error (%)
1	-0.01909	-0.01898	0.58
2	-0.02344	-0.02370	1.11
3	-0.01828	-0.01764	3.52
4	-0.01284	-0.01338	4.24

Table 4. Data Comparison

After calculating coefficients W_0, ρ, β, the Gumbel probability density curve and the slope of the curve at any point can be determined.

3.2 Coefficients Backcalculation Using Correspondence Principle

A beam-on-elastic foundation solution is introduced in the previous sections. Also, transformation of the solution from elastic to viscoelastic and application of the approximate inverse Laplace Transform method have been introduced. Deflections of the points where lasers are set can be expressed as in Figure 11.

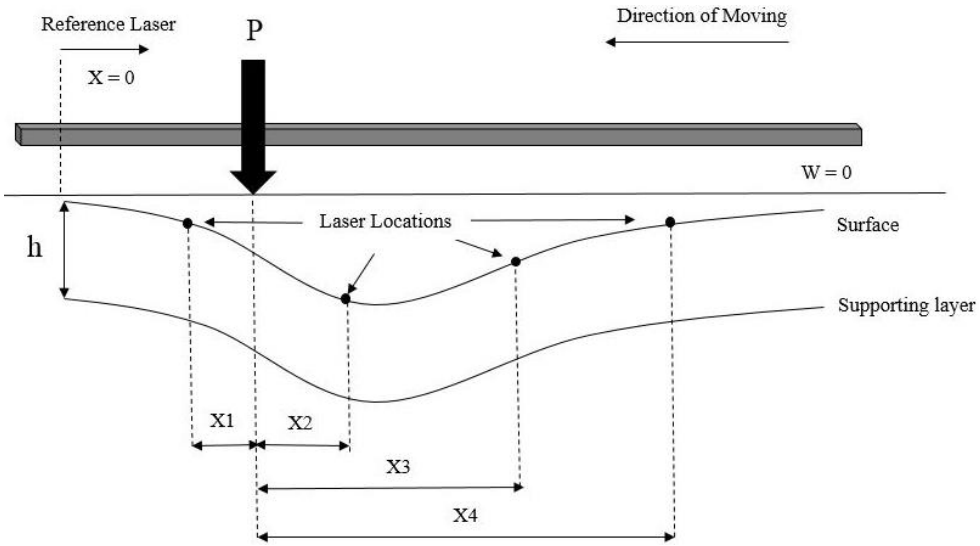

Figure 11. Locations of Lasers and Loads

h is the thickness of the surface, $x_1 \sim x_4$ are distances of lasers and the location where the load acts. Denote v as the velocity of the vehicle. Based on Hetenyi's solution (Hetenyi 1946), express the deflection values and the slope of the deflection basin under static loads as

$$w(x) = Ae^{-\beta x}\cos\beta x + Be^{-\beta x}\sin\beta x + q/k \tag{53}$$

$$w'(x) = \beta(B-A)e^{-\beta x}\cos\beta x - \beta(B+A)e^{-\beta x}\sin\beta x \tag{54}$$

then change terms β, k with those in Equation (48) and (49) to obtain $w(x,t), w'(x,t)$,

$$w(x_i,t) \cong \left[s_i w(s_i,t) \right]_{s_i=1/2t_i} \tag{55}$$

$$w'(x_i,t) \cong \left[s_i w'(s_i,t) \right]_{s_i=1/2t_i} \tag{56}$$

$$t_i = \frac{x_i}{v} \tag{57}$$

Four lasers can provide data $w(x_1,t) \sim w(x_4,t)$, and the fitted Gumbel probability density curve can provide $w'(x_1,t) \sim w'(x_4,t)$. Eight data are enough for solving six unknown coefficients A, B, E_1, E_2, m_1, m_2.

The analysis described above also requires the thickness h of the pavement surface layer that can be determined with sufficient accuracy by an accompanying Ground Penetrating Radar (GPR) survey. Both the moving deflection basin and the GPR surface layer thickness will be coordinated with the on-board sub-meter accuracy of GPS equipment.

4 SIMULATION RESULTS*

4.1 Construction of Finite Element Models

The objectives of building numerical models using a finite element software (ABAQUS 1989) are:

- Due to the complexity of the problem and lack of insitu testing data, a finite element software is essential for obtaining deflection data of the surface of the pavement to backcalculate properties of materials.
- The shape of a deflection basin is affected by various factors such as the speed of loading, material properties and so on. A finite element software can effectively control input variables for researchers to figure out how those variables influence the shape individually.
- Based on previous assumptions and analysis, loading with highway-speed is of necessity to replace current stationary FWD loads from two aspects: getting rid of traffic control and providing more information for evaluation and prediction of the pavement. A finite element software can provide cases with different loading speeds, which give a straightforward comparison of deflection basins at different loading speeds.

For convenience of modeling and calculation, the numerical models and simulation of a moving vehicle are simplified in terms of the following aspects:

1. The whole pavement structural system is divided into three layers, of which the

*Reprinted with permission from Carlson, Paul, et al. *Advancing Innovative High-Speed Remote-Sensing Highway Infrastructure Assessment Using Emerging Technologies*. No. FHWA/TX-16/0-6869-1. 2017.

top is the surface of the pavement, the middle is the base course and the bottom is the subgrade course. The thickness of the three layers are 4 in, 6 in and 70 in. Such a layer arrangement is representative of typical flexible pavements. The thickness of the subgrade course is set to be much greater than the surface to represent a semi-infinite course.

2. Contact areas of tires and pavement surface are assumed to be two identical rectangles which represent two parallel tires. The size of one is 8.4×7.2 in. The tire contact pressure is assumed to be a uniform pressure, of which the value is 100 psi.
3. The movement of vehicles can be represented by consecutive loading steps in which the locations of the loading areas are changed with time. For precision of the modelling, one contact area is divided into three parts in the moving direction. The length of each step equals the time vehicles travel at the distance of one part at a given speed. The conceptual sketch of load moving is illustrated in Figure 12.

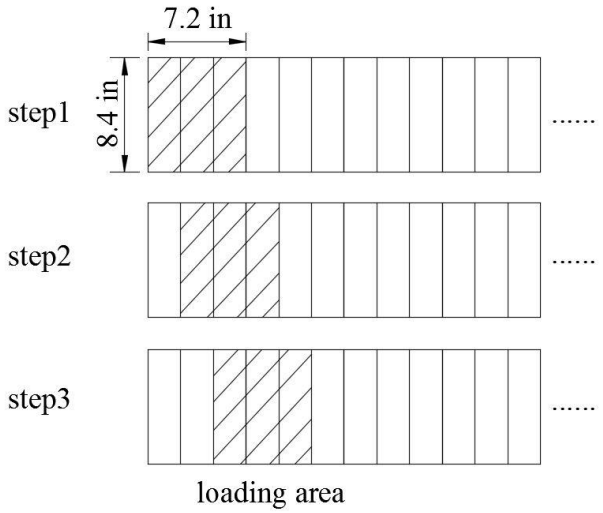

Figure 12. Simulation of Moving Load

4. The mesh size of the system is determined by dimensions of different sections. For loading sections, the mesh size coincides with the width and length of the contact area. For other sections, mesh sizes are adjusted based on dimensions of sections to maintain a reasonable ratio for each element. Figure 13 shows a model after meshing.

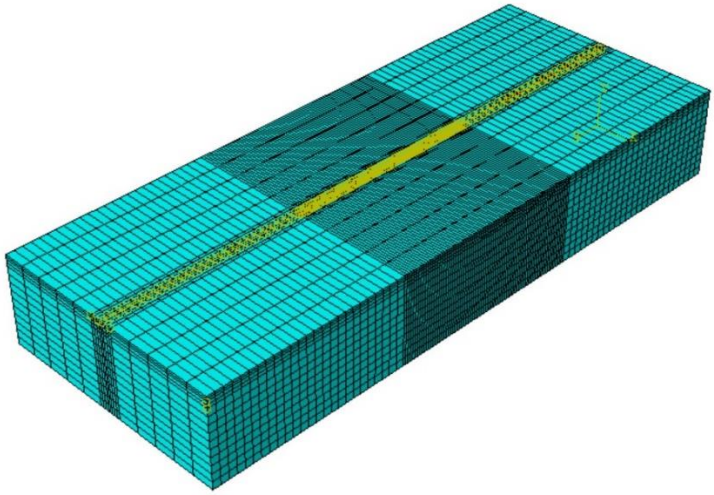

Figure 13. Numerical Model after Meshing

4.2 Material Properties

In order to represent trends of the phase angle and modulus representing pavement materials in their life cycles. Three typical sets of viscoelastic surfaces and base courses are created as Table 5. The subgrade is set to be an elastic material of which the elastic modulus is 4.5 ksi.

$E(t) = E_1 t^{-m}$		Type 1	Type 2	Type 3
Surface	E_1 (ksi)	41.453	76.028	123.210
	m	0.449	0.368	0.250
	ϕ (degree)	40.41	33.12	22.50
Base	E_1 (ksi)	7.96	15.761	28.925
	m	0.533	0.456	0.363
	ϕ (degree)	47.97	41.04	32.67

Table 5. Coefficients of Three Flexible Pavements

Equation (6) expresses the modulus as time-dependent and Equation (9) ~ (12) describe Prony series. By adjusting values in Prony series, different modulus and m can be obtained. For example, input instantaneous modulus and Prony series coefficients as Table 6, an equivalent power law function for the material is defined as in Figure 14.

i	$\tau_i\,(s)$	g_i, k_i	$E_i^a\,(ksi)$	E_∞^a (ksi)	$E_0\,(ksi)$
1	4.09E-06	0.3620	1267.000	8.05	3500
2	2.56E-04	0.3630	1270.500		
3	7.71E-03	0.1765	617.750		
4	2.10E-01	0.0740	259.000		
5	3.88E+00	0.0165	57.750		
6	6.53E+01	0.0057	19.950		

Table 6. Prony Series and Instantaneous Modulus of Surface (Type 2)

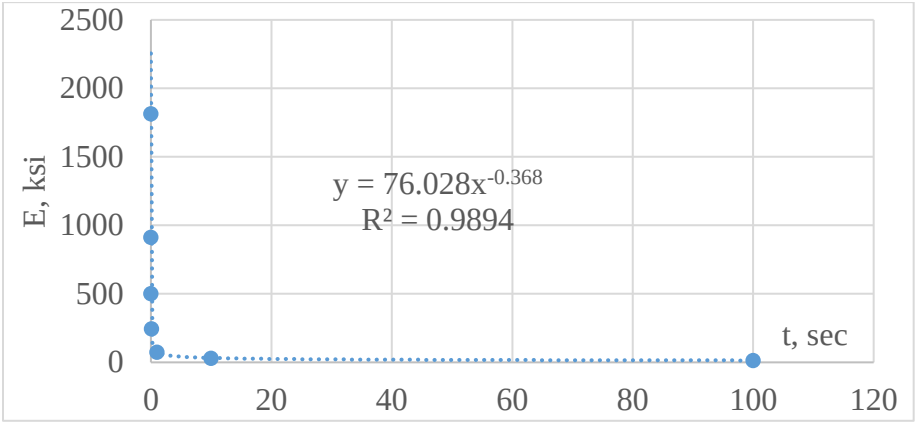

Figure 14. Fitted Power-Law Function with Prony-Series Data of Surface (Type 2)

Other Prony series data and fitted curves are shown in the Appendix.

Besides viscoelasticity of materials, basic information defining the surface and base inertial damping are input into ABAQUS.

Basic Properties of Surface	Density (lbf s^2/in^4)	0.0002098
	Rayleigh Inertial Damping Ratio (Alpha)	0.93
	Rayleigh Inertial Damping Ratio (Beta)	0.0027

Table 7. Basic Properties of Surface

Basic Properties of Base	Density (lbf s^2/in^4)	0.0001798
	Rayleigh Inertial Damping Ratio (Alpha)	0.41
	Rayleigh Inertial Damping Ratio (Beta)	0.0061

Table 8. Basic Properties of Base

Table 7 and Table 8 show basic inertial damping of asphalt surface and base. The effects of dynamic properties of pavements on responses have been introduced in previous sections. This thesis compares two analyzing methods in ABAQUS: the first one considers viscoelasticity of materials as well as inertial damping ratios which reflect conditions of whole system while the other one eliminates the inertial damping to show effects of moving loads on deflection basins due to viscoelasticity of materials only. This assumption can be achieved using ‘Visco’ and ‘Dynamic’ types of analysis methods

individually in ABAQUS, of which the previous one is used when inertial effects can be neglected (ABAQUS 2010).

4.3 Results of Simulation

4.3.1 Results of 'Visco' Analysis

Comparison of the deflection basins caused by loads of different velocities in Figure 20 shows that velocities of moving loads affect not only the values of the deflection but also shift the distance between the location of the maximal deflection and the location of the load or the trailing reference point. It can be seen that:

1. With the increase of speed, the maximum deflection will decrease;
2. There exists a lag distance between locations where the load acts and the maximum deflection occurs;
3. With the increase of speed, the distance between the locations of maximum deflection and the reference point will also increase.

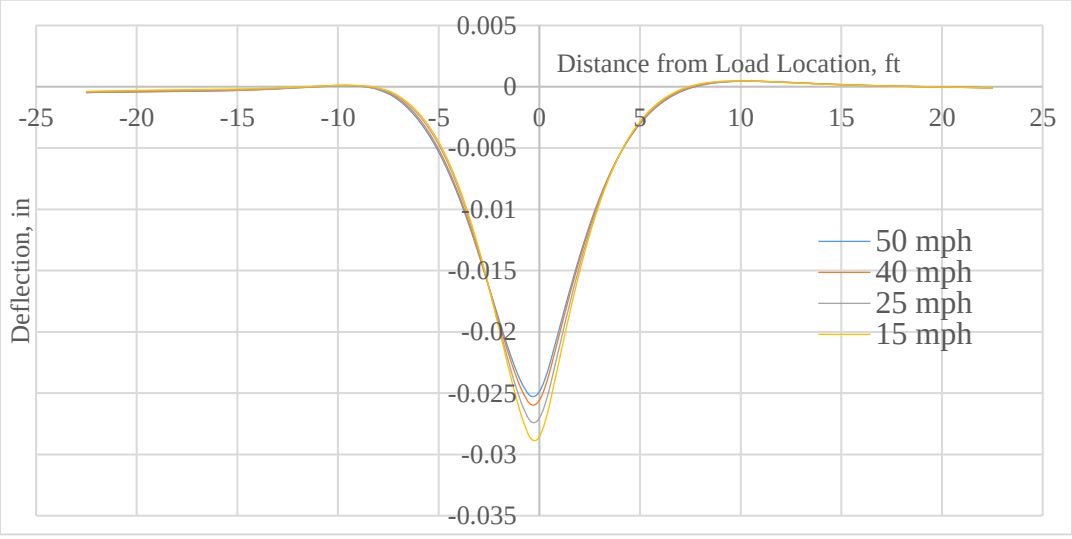

Figure 15 (a)-(c) Pavement Type 1 under Different Moving Loads Using 'Visco' Analysis

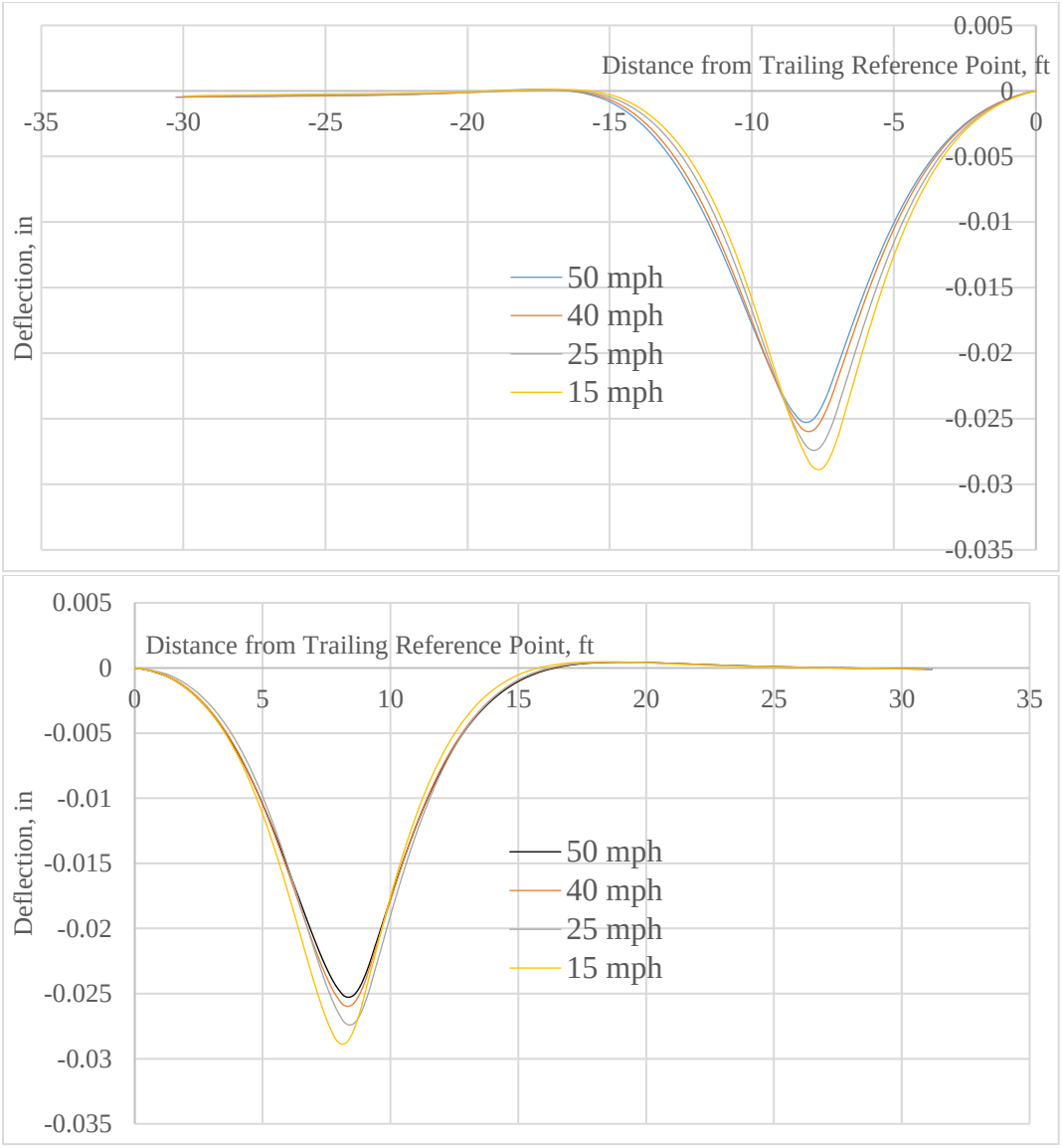

Figure 15 (a)-(c) Continued

Deflection basins of other two types of pavements under different moving loads are shown in the Appendix.

Deflection basins of different pavements under the load moving at 50 mph in Figure 15 show the responses of pavements under different loading cycles. Changing from material Type 3 to material Type 1 represents the increasingly deteriorated pavements of which the modulus decreases while the phase angle increases. From Figure

16, it can be seen that with increasing deterioration of pavements, the magnitude of deflection will increase and the lag distance from the location of maximum deflection to the location of the load and the trailing reference point will increase.

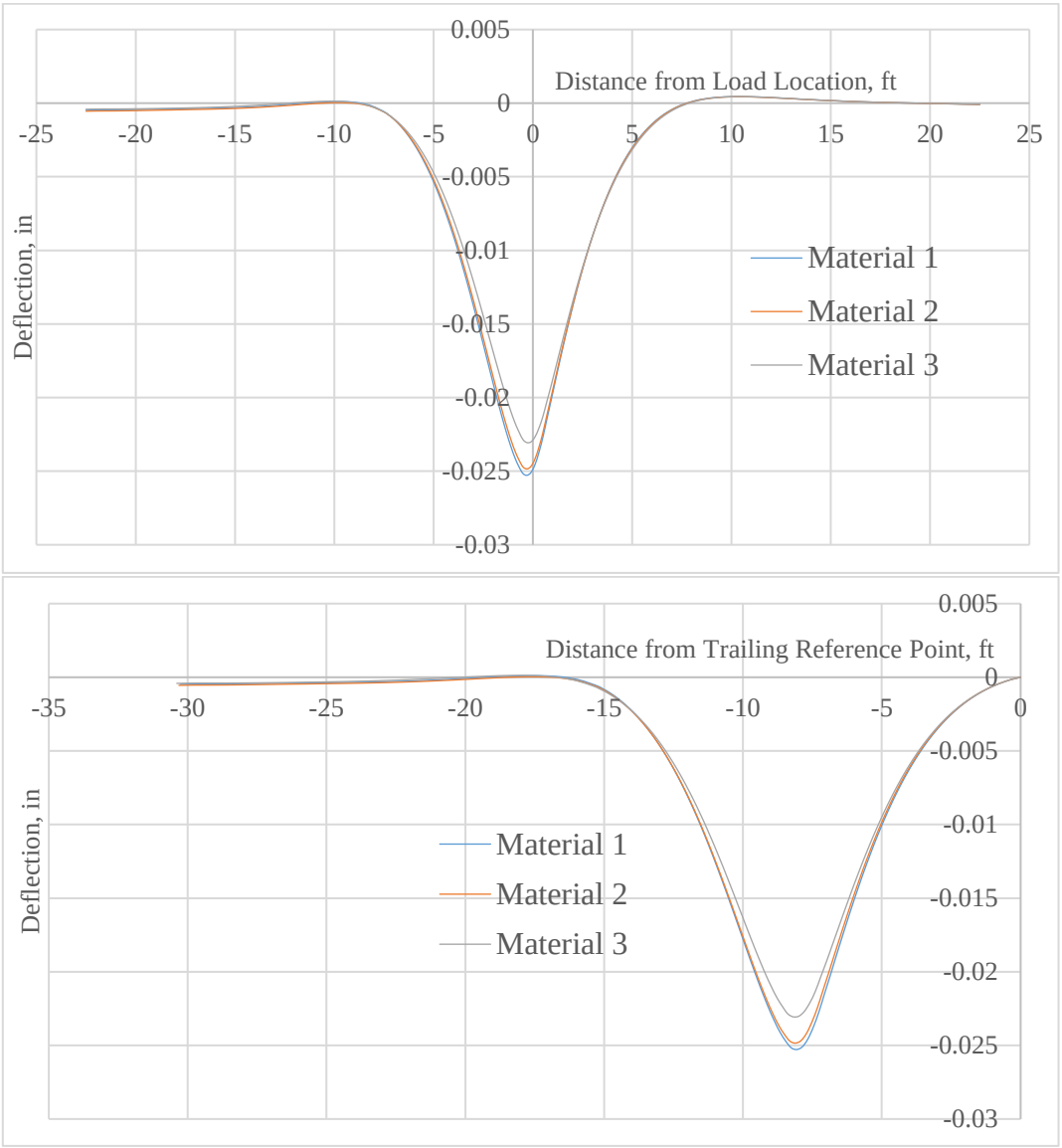

Figure 16 (a)-(b) Pavements under Moving Loads v= 50mph Using 'Visco' Analysis

Comparison of deteriorating pavements under other moving loads are shown in Appendix.

4.3.2 Results of 'Dynamic' Analysis

For simulating pavement structural system in real conditions, cases including inertial damping are shown in this section. It is assumed that the deterioration of pavement has no effects on the value of its inertial damping ratio. Similarly, Pavement Type 1 under different moving loads and comparison of deteriorating pavements under the load moving at 50 mph are presented in Figure 17 and Figure 18.

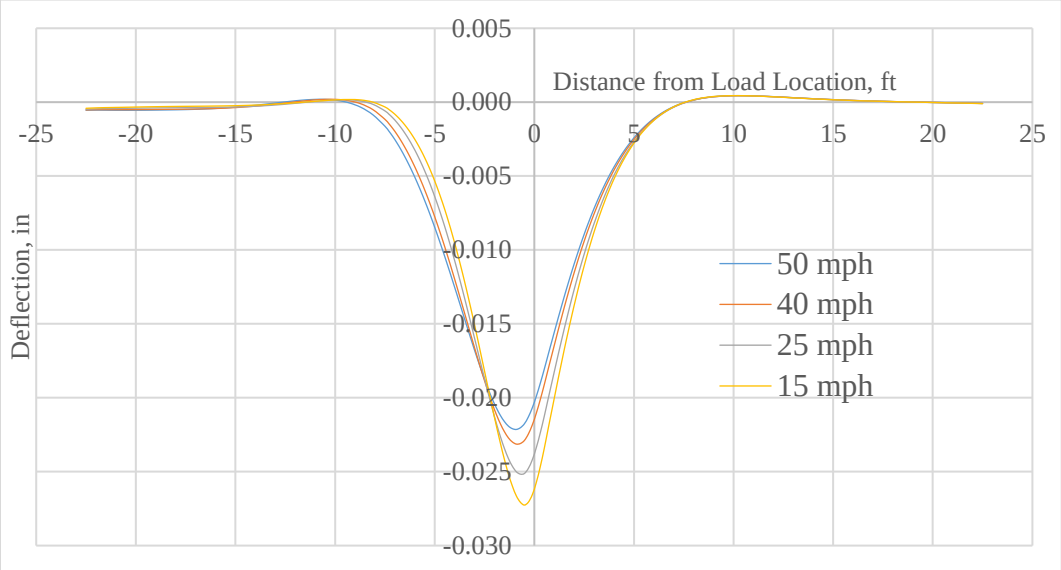

Figure 17 (a)-(c) Pavement Type 1 under Different Moving Loads Using 'Dynamic' Analysis

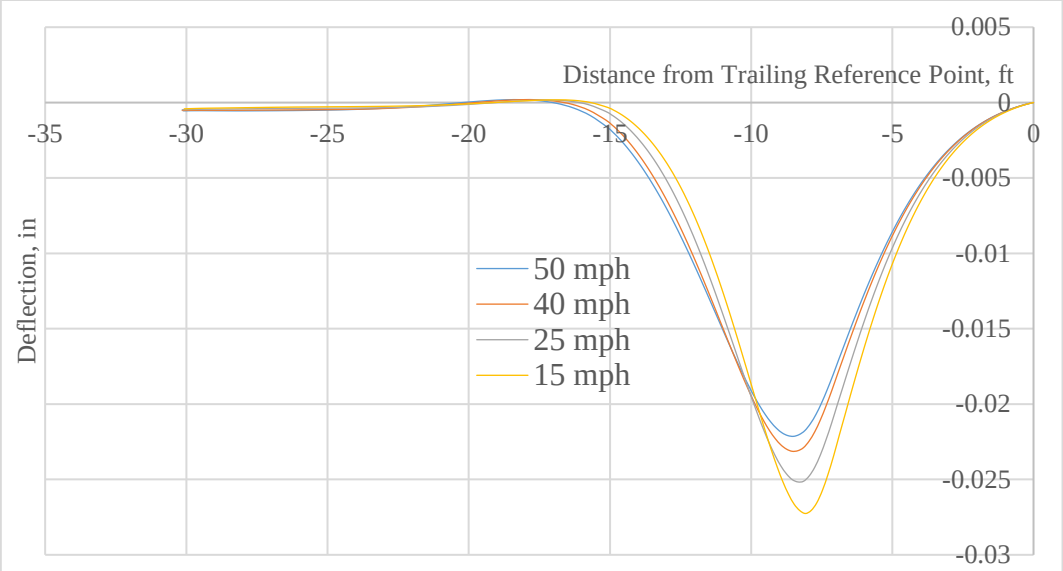

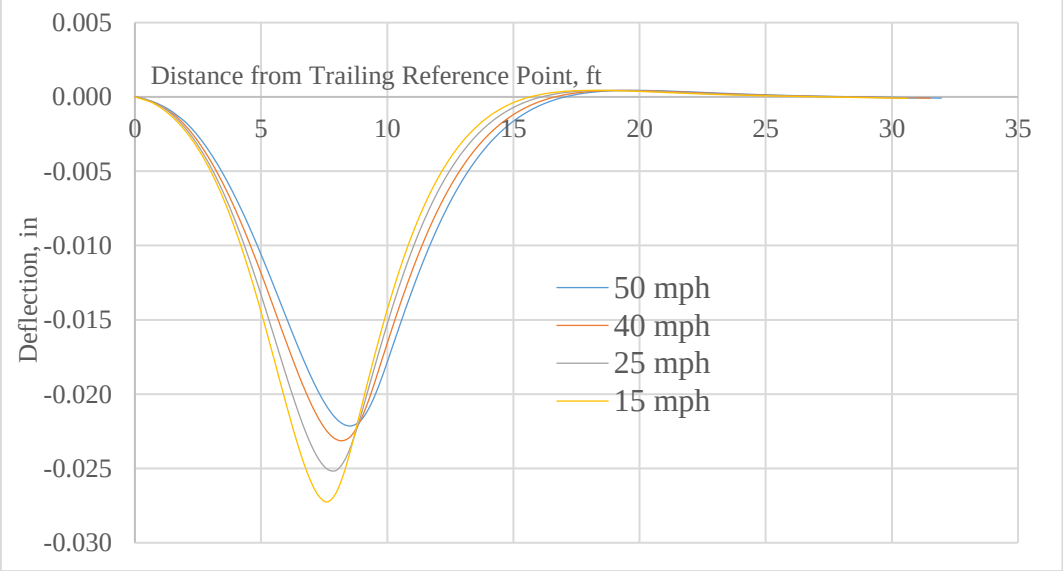

Figure 17 (a)-(c) Continued

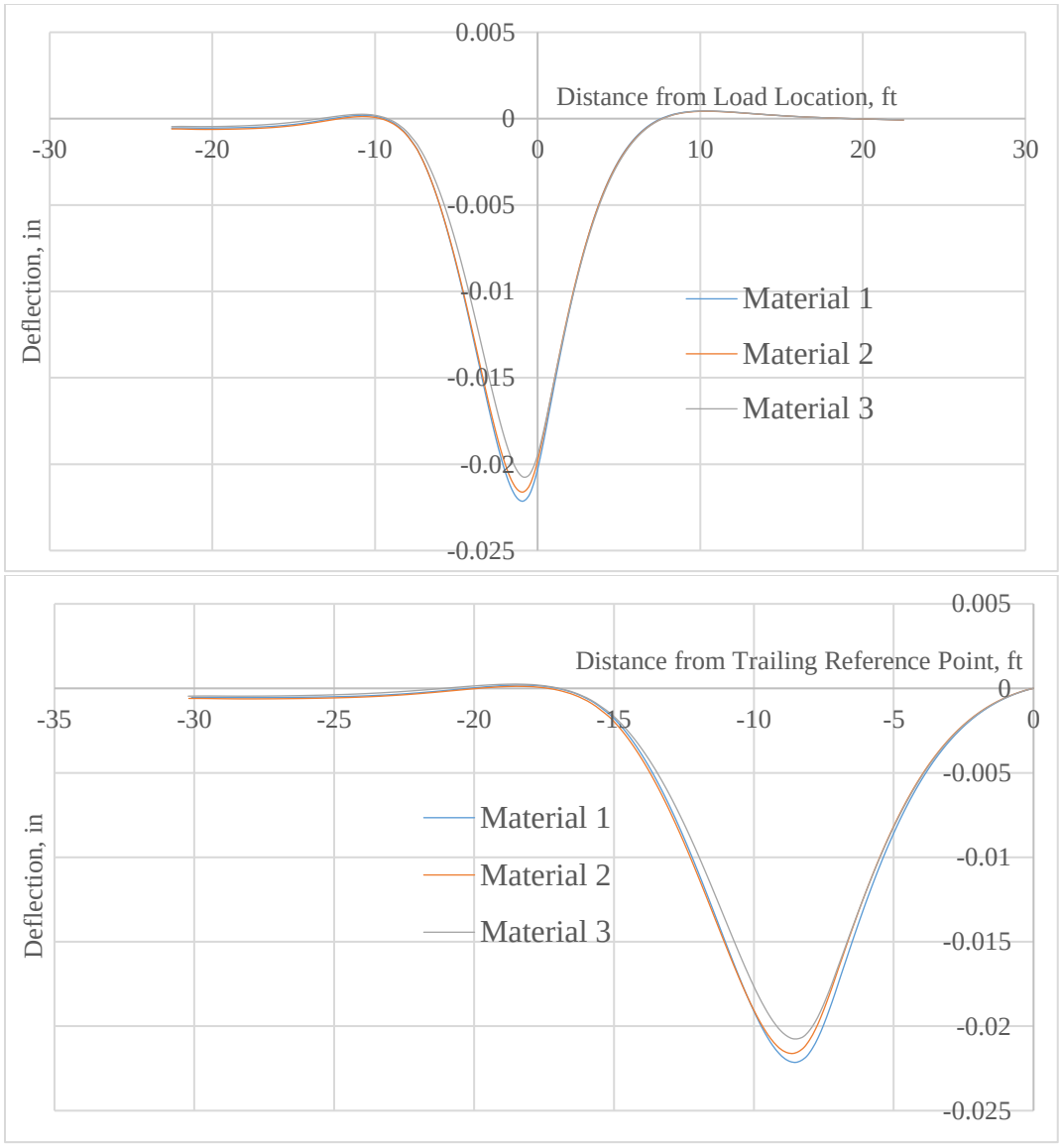

Figure 18 (a)-(b) Pavements under Moving Loads v= 50mph Using 'Dynamic' Analysis

Other cases are shown in Appendix.

The results of cases considering inertia damping of the pavement are similar to those of cases focusing on the viscoelasticity of materials. Moreover, the shift distance is more obvious. In order to show effects of inertia damping, pavement Type 1 under moving load of 50 mph using 'visco' and 'dynamic' analysis methods presented in Figure 19 and Figure 20.

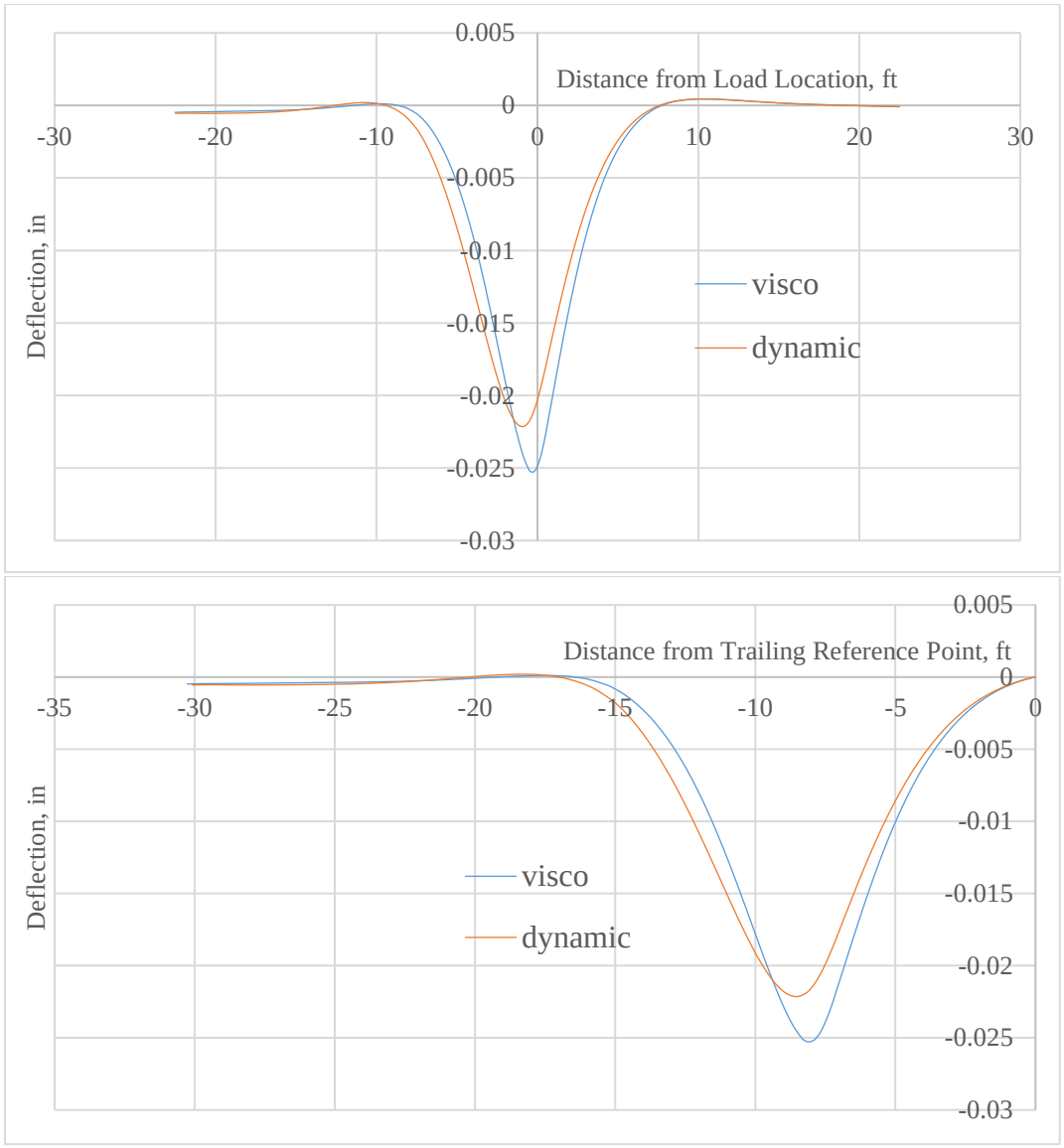

Figure 19 (a)-(b) Pavement Type 1 under Moving Loads v=50 mph with/without Inertia Damping

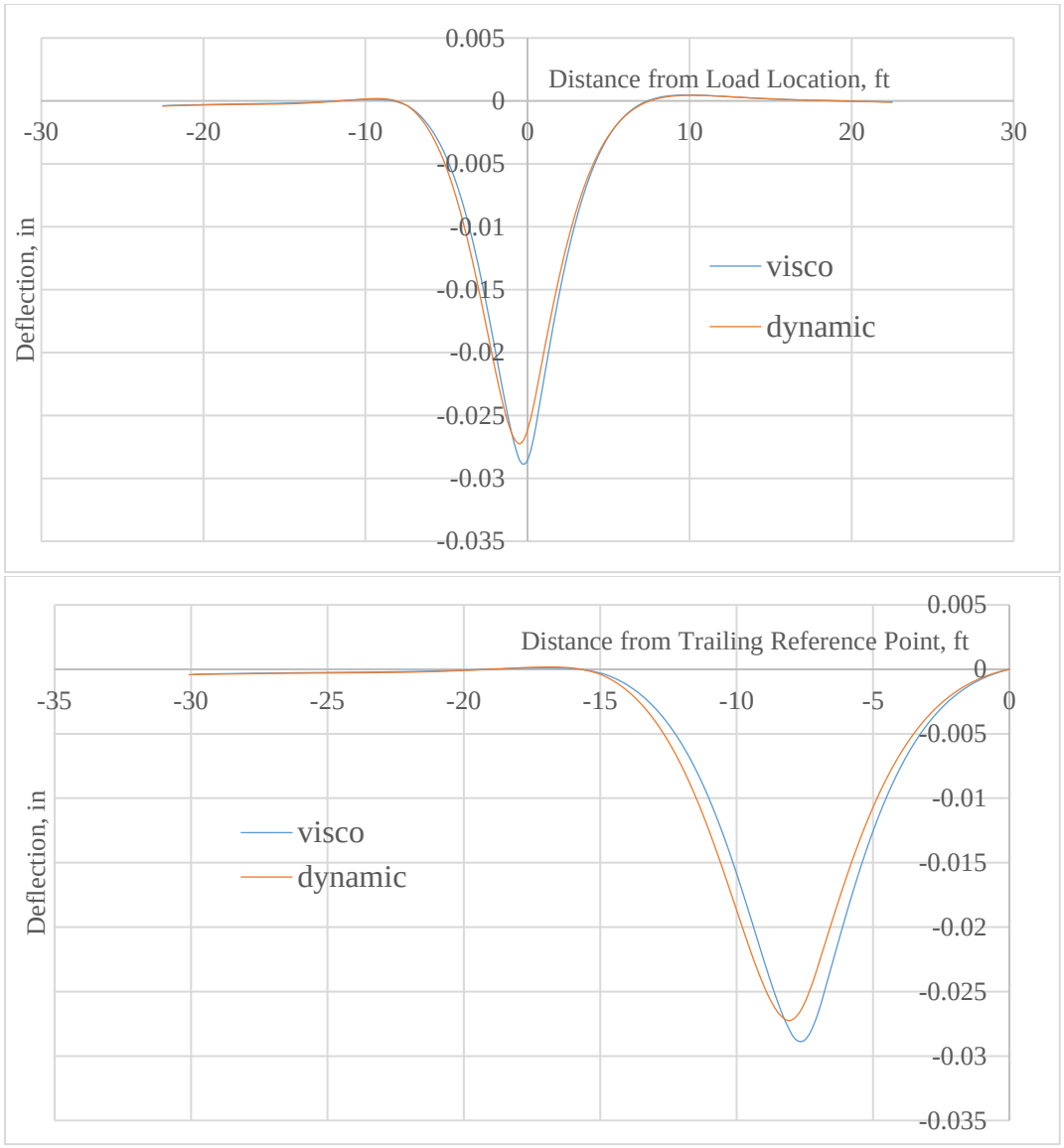

Figure 20 (a)-(b) Pavement Type 1 under Moving Loads v=15 mph with/without Inertia Damping

It shows that inertia damping reduces the magnitude of deflections and increase the lag distance. Hence, it can be concluded that the asymmetry of the deflection basin is caused by both the viscoelasticity and inertia damping of pavement materials.

5 SUMMARY AND CONCLUSIONS*

5.1 Capabilities of New Concept

Based on the work that has been accomplished in this thesis, there are following findings:

- The literature review reveals that the current deflection measurement systems generally consist of two types: stationary (like FWD) or travelling slowly (like RDD and TPAD) and dynamic (like RWD). The RDD, TPAD and RWD are limited for their lack of accuracy and can only be used for qualitative evaluation using averaged or maximum deflection data. The analysis of the FWD testing is able to output material properties of pavement layers. However, the operational time of the testing significantly increases costs and risks.
- The proposed highway speed deflection basin-pavement material property measuring system uses a new concept of measuring the shape of the deflection basin instead of just the values of a single deflection, based on which the viscoelastic properties of the pavement layers can be calculated in addition to the elastic properties in the existing back-calculation approaches that are used with the FWD.
- The results of numerical models show the effects of speeds on the shapes of the deflection basins. Also, it shows the effects viscoelasticity and inertial damping on the shapes of the deflection basins. Such results demonstrate the sensitivity with

*Reprinted with permission from Carlson, Paul, et al. *Advancing Innovative High-Speed Remote-Sensing Highway Infrastructure Assessment Using Emerging Technologies*. No. FHWA/TX-16/0-6869-1. 2017.

which a moving deflection basin can detect reliably the rate of deterioration of an asphalt pavement. Measuring this rate in the early stages of deterioration will give an advanced warning of when severe pavement cracking will occur and will give pavement network managers the necessary lead time to plan and executive timely cost-effective maintenance practices.

5.2 Future Work

The future work of the theoretical parts of this new methodology includes:

- Finalize the backcalculation analytical process for coefficients in the model of 'beams on viscoelastic foundation' to prove the accuracy of this theoretical model.
- Make ABAQUS runs using pavement layer properties for intact and deteriorated pavements to verify the accuracy of the backcalculation process and sensitivity of this model to changes of pavement properties.
- Discuss whether it is necessary to convert the analytical backcalculation process into artificial neural network models.

REFERENCES

ABAQUS. *ABAQUS, Finite Element Computer Program*, Hilbert, Karlsson and Soreson, Inc, 2010.

Andr´en, P. and C. A. Lenngren. Evaluating pavement layer properties with a high-speed rolling deflectometer. In A. K. Mal (Ed.), *Nondestructive Evaluation of Aging Aircraft, Airports and Aerospace Hardware IV Proceedings*, Volume 3994, Newport Beach, CA, USA, pp. 192–200. SPIE—The International Society for Optical Engineering, 2000.

Arora, J., Nazarian, S., and Tandon, V. *Continuous Deflection Testing of Highways at Traffic Speeds*. Research Report 0-4380-1, Center for Transportation Infrastructure Systems, The University of Texas at EI Paso, EI Paso, 2006.

Bay, James Anderson, and I. I. Stokoe. *Development of a rolling dynamic deflectometer for continuous deflection testing of pavements*. No. FHWA/TX-99/1422-3F,. 1998.

Biot MA. *Bending of An Infinite Beam on An Elastic Foundation*. Zeitschrift fiir Angewandte Maihematik und Mechanik. 1922 Jun;2(3):165-84.

Briggs, R. C., Johnson, R. F., Stubstad, R. N., and Pierce, L. *A Comparison of the Rolling Weight Deflectometer with the Falling Weight Deflectometer*. Nondestructive Testing of Pavements and Backcalculation of Moduli: Third Volume, ASTM STP 1375, S. D. Tayabji and E. O. Lukanen, Eds., American Society for Testing and Materials, West, Conshohocken, PA, 1999.

Cost, Thomas L. *Approximate Laplace Transform Inversions in Viscoelastic Stress Analysis*. AIAA Journal 2, no. 12 (1964): 2157-2166.

Gay, Derek A. *Development of a Predictive Model for Pavement Roughness on Expansive Clay*. Ph.D. dissertation, Texas A&M University, 1994.

Hall, Jim W., and Steele, Douglas A. *Rolling Wheel Deflectometer (RWD) Demonstration and Comparison to Other Devices in Texas.* ERES Consultants, 2004.

Herr W, Halla JW. Jr, White TD, Johnson W. *Continuous Deflection Basin Measurement and Backcalculation under a Rolling Wheel Load Using Scanning Laser Technology*. Proc. of The Transportation Congress, Vol. 1, pp. 600-611.

Hetenyi, M. *Beams on Elastic Foundation*. The University of Michigan Press, Ann Arbor, 1946.

Hildebrand, Gregers, and Rasmussen, Søren. *Development of a High Speed Deflectograph*, Road Directorate, Denmark, 2002.

Jitin, Arora, Vivek Tandon, and Soheil Nazarian. *Continuous Deflection Testing of Highways at Traffic Speeds*. No. FHWA/TX-06/0-4380-1. 2006.

Lakes, Roderic S. *Viscoelastic Materials*. Cambridge University Press, 2009. LMI Technologies. *Gocator All-in-One 3D Smart Sensor*. http://lmi3d.com/sites/default/files/BROCHURE_Gocator_3D-Smart-Sensors2.4_WEB.pdf. Accessed December 10, 2015.

Lytton, R., *Backcalculation of Pavement Layer Properties*, Nondestructive Testing of Pavements and Backcalculation of Moduli, STP19797S, G. Baladi and A. Bush, Ed., ASTM International, West Conshohocken, PA, 1989, pp. 7-38.

MATLAB. R2015a, The MathWorks Inc., Natick, MA, 2015.

Pipkin, Allen C. *Lectures on viscoelasticity theory*. Vol. 7. Springer Science & Business Media, 2012.

Reese, Ronald. "Properties of aged asphalt binder related to asphalt concrete fatigue life." *Journal of the Association of Asphalt Paving Technologists* 66 (1997).

Schapery, R. A. A theory of crack initiation and growth in viscoelastic media. *International Journal of Fracture* 11.1, 1975, pp. 141-159.

Schapery, R.A. *Correspondence Principles and a Generalized J Integral for Large Deformation and Fracture Analysis of Viscoelastic Media*. International Journal of Fracture, Vol. 25, No. 3, 1984, pp. 195–223.

Steele, D. A., and W. R. Vavrik. "Rolling Wheel Deflectometer (RWD) Demonstration and Comparison to Other Devices in Texas." *ARA Project* 15874 (2004).

Terzaghi K. *Evaluation of Coefficients of Subgrade Reaction*. Geotechnique. 1955 Dec;5(4):297-326.

TxDOT, *Technical Advisory: Frequently Asked Questions about the Falling Weight Deflectometer (FWD).* ftp://ftp.dot.state.tx.us/pub/txdotinfo/cst/tips/falling_weight_deflectometer.pdf. Accessed December 10, 2015.

Vesic AB. *Bending of Beams Resting on Isotropic Elastic Solid*. Journal of the Engineering Mechanics Division. 1961 Apr;87(2):35-54.

Wineman, Alan S., and Kumbakonam Ramamani Rajagopal. *Mechanical Response of Polymers: An Introduction*. Cambridge University Press, 2000.

APPENDIX A

PRONY DERIES AND FITTED POWER-LAW FUNCTIONS

i	$\tau_i\,(s)$	$g_i\,,k_i$	$E_i^a\,(ksi)$	E_∞^a (ksi)	E_0 (ksi)
1	4.09E-06	0.3620	1448	15	4000
2	9.22E-06	0.1000	400		
3	2.08E-02	0.0791	316.500		
4	5.12E-01	0.0276	110.579		
5	6.99E+00	0.0126	50.383		
6	1.21E+02	0.0097	38.852		

Table A.1 Prony Series and Instantaneous Modulus of Surface (Type 3)

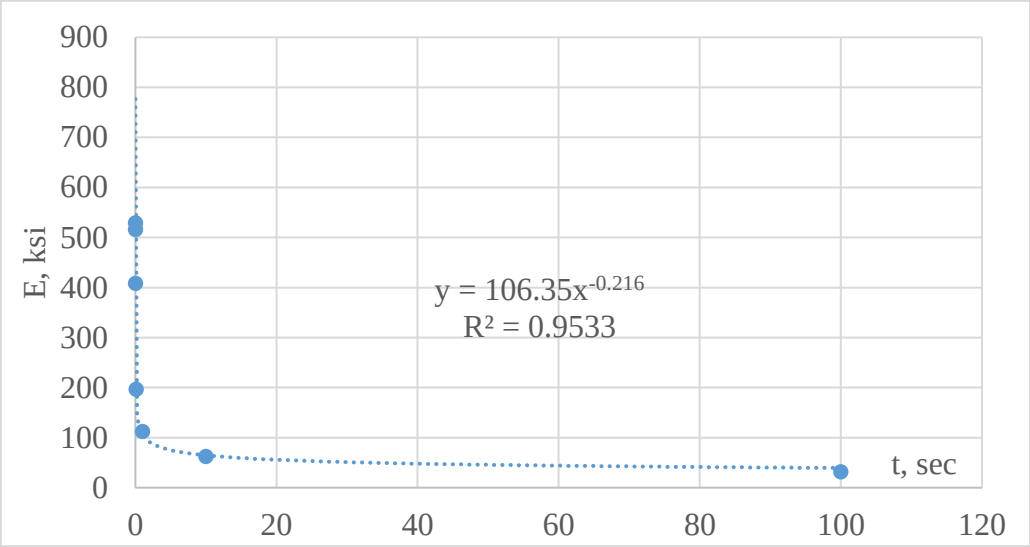

Figure A.1 Fitted Power-law Function with Prony-Series Data of Surface (Type 3)

i	$\tau_i\,(s)$	$g_i\,,k_i$	$E_i^a\,(ksi)$	E_∞^a (ksi)	E_0 (ksi)
1	4.09E-06	0.3632	955.216	0.263	2630
2	1.28E-05	0.1000	263.000		
3	5.50E-03	0.2645	695.631		
4	1.39E-01	0.0586	154.075		
5	3.00E+00	0.0141	37.196		
6	8.66E+01	0.0048	12.641		

Table A.2 Prony Series and Instantaneous Modulus of Surface (Type 1)

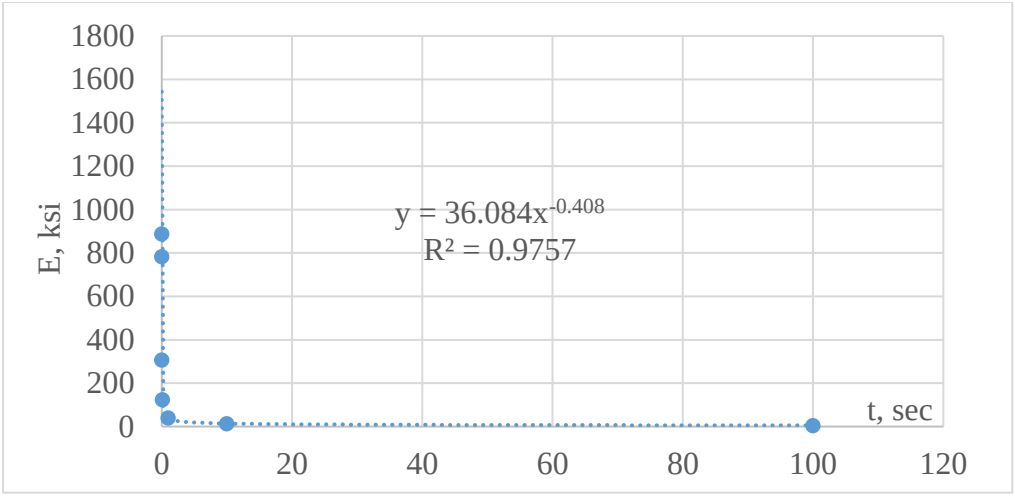

Figure A.2 Fitted Power-law Function with Prony-Series Data of Surface (Type 1)

i	$\tau_i\,(s)$	g_i, k_i	$E_i^a\,(ksi)$	E_∞^a *(ksi)*	E_0 *(ksi)*
1	0.0014	0.9059	724.72		
2	0.0123	0.256	204.8		
3	0.1141	0.0706	56.48	0.7396	800
4	1.1981	0.0182	14.56		
5	15.29	0.0045	1.6		

Table A.3 Prony Series and Instantaneous Modulus of Base (Type 1)

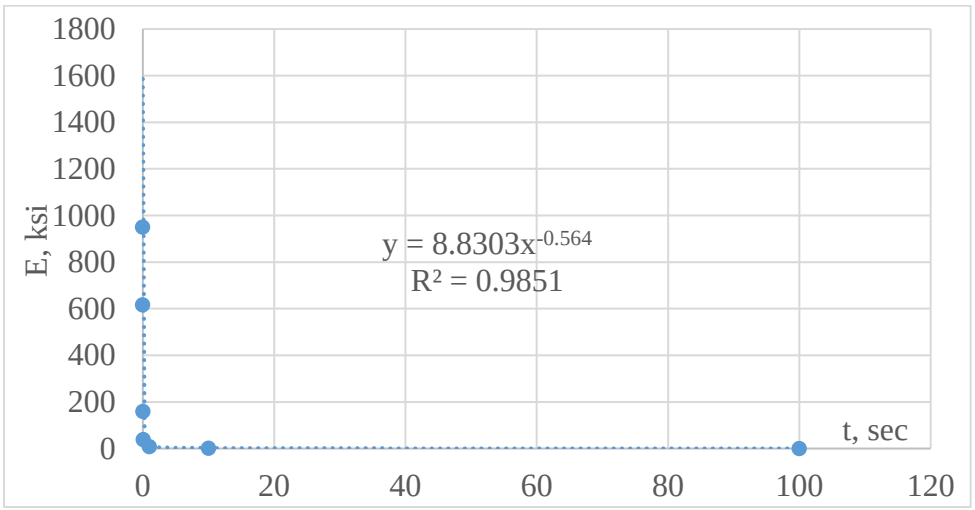

Figure A.3 Fitted Power-law Function with Prony-Series Data of Base (Type 1)

i	$\tau_i\,(s)$	g_i, k_i	$E_i^a\,(ksi)$	E_∞^a (ksi)	E_0 (ksi)
1	0.0019	0.6072	485.76		
2	0.019	0.1882	150.56		
3	0.1898	0.0595	47.6	1.6913	800
4	1.8977	0.0189	15.12		
5	20.93333	0.0066	5.28		

Table A.4 Prony Series and Instantaneous Modulus of Base (Type 2)

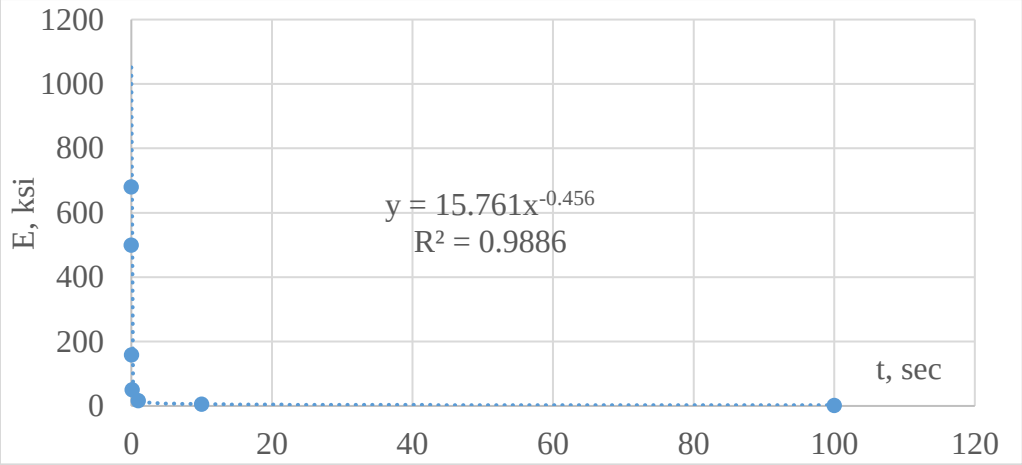

Figure A.4 Fitted Power-law Function with Prony-Series Data of Base (Type 2)

i	$\tau_i\,(s)$	g_i, k_i	$E_i^a\,(ksi)$	E_∞^a (ksi)	E_0 (ksi)
1	0.0026	0.4667	373.36		
2	0.0305	0.1625	130		
3	0.3106	0.0609	48.72	4.69	800
4	2.8247	0.0242	19.36		
5	27.2709	0.0117	9.36		

Table A.5 Prony Series and Instantaneous Modulus of Base (Type 3)

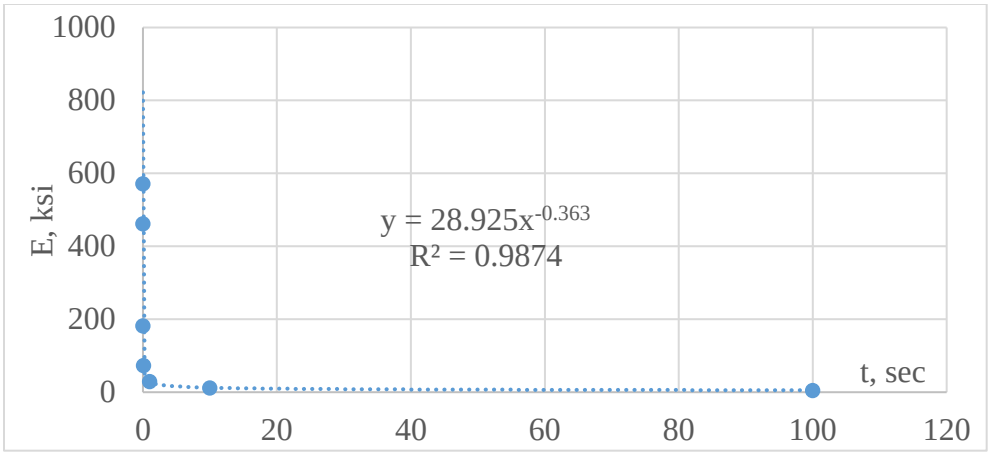

Figure A.5 Fitted Power-law Function with Prony-Series Data of Base (Type 3)

APPENDIX B

DEFLECTION BASINS OF 'VISCO' ANALYSIS

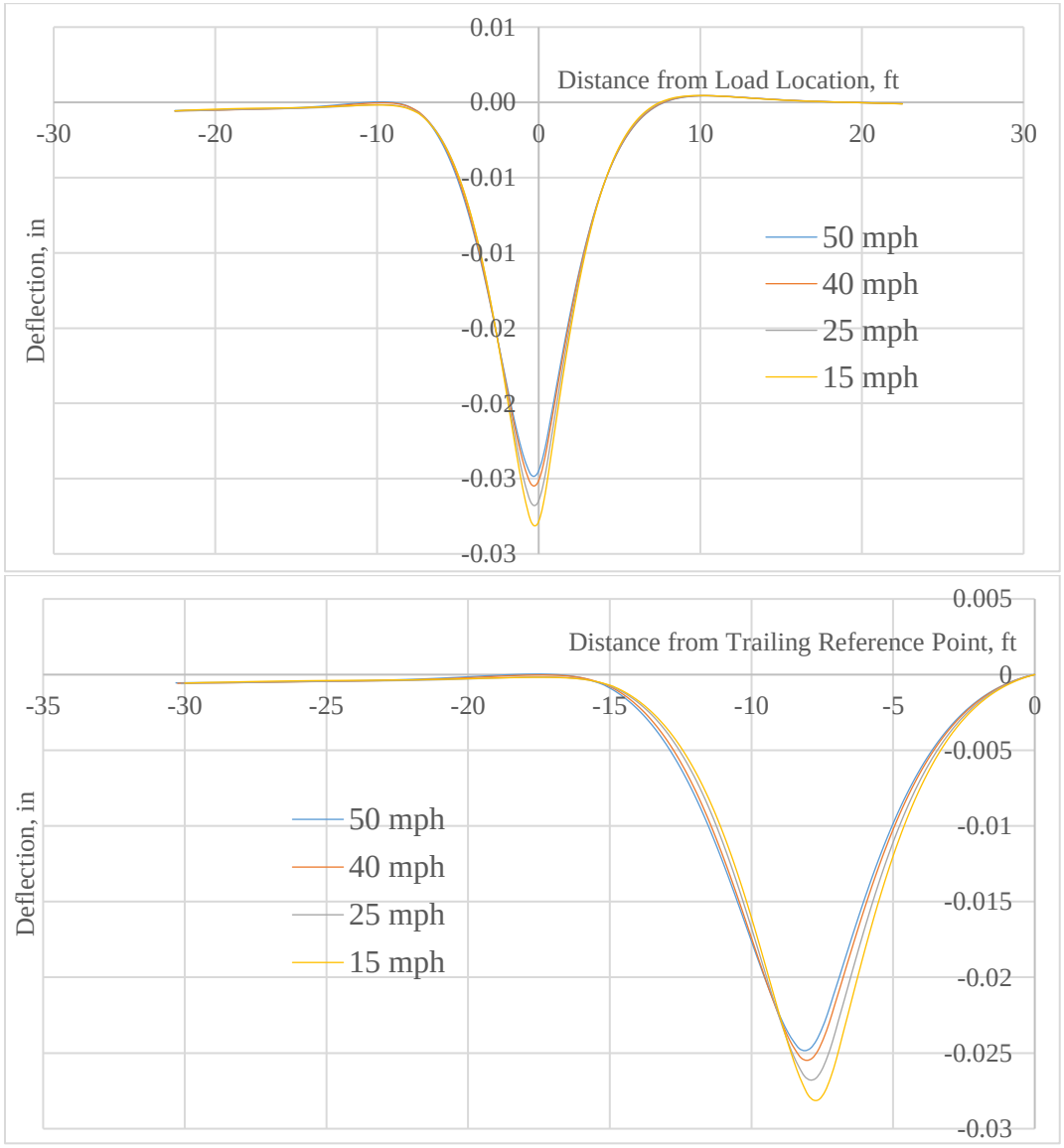

Figure B.1 (a)-(b) Pavement Type 2 under Different Moving Loads Using 'Visco' Analysis

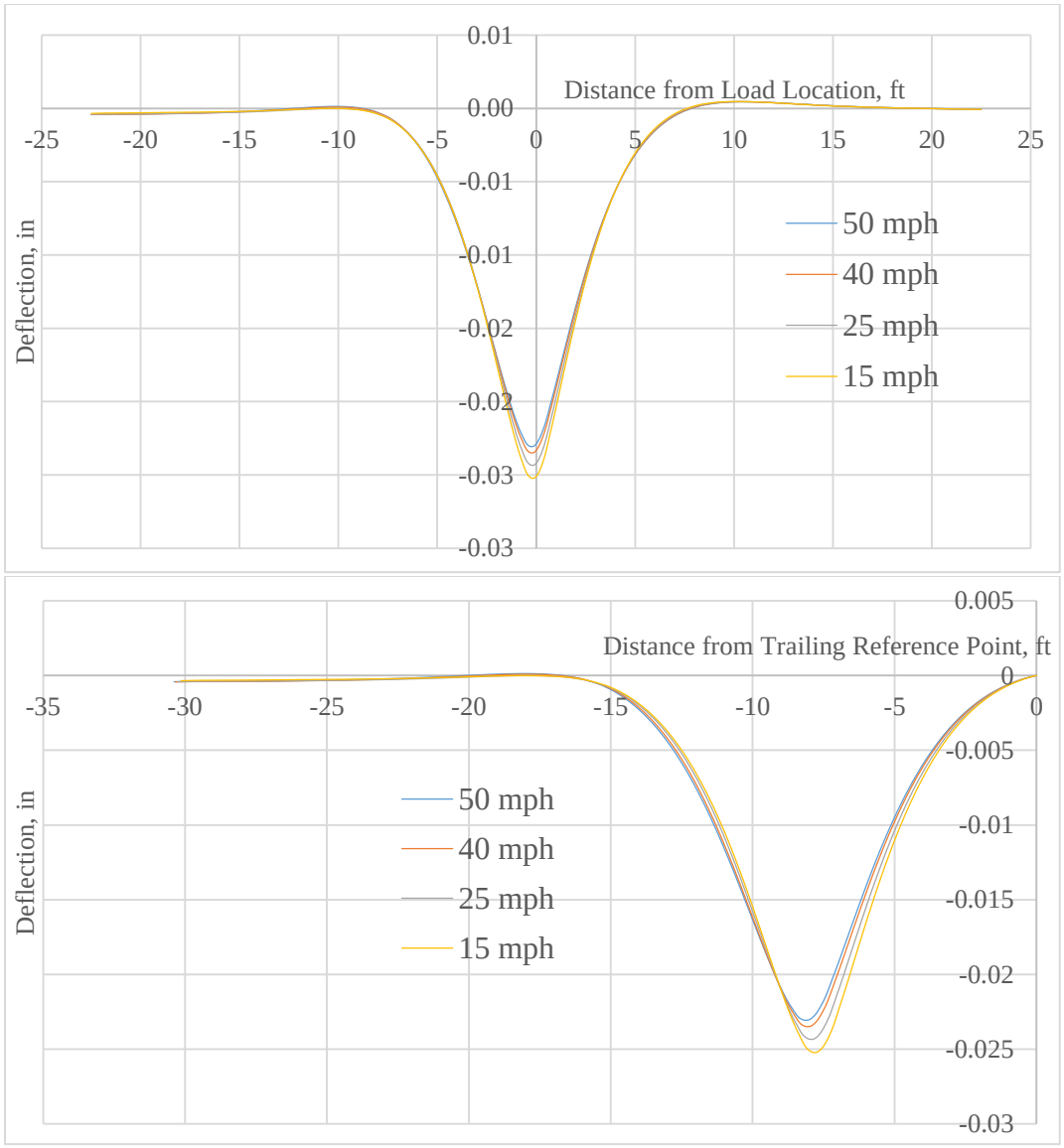

Figure B.2 (a)-(b) Pavement Type 3 under Different Moving Loads Using 'Visco' Analysis

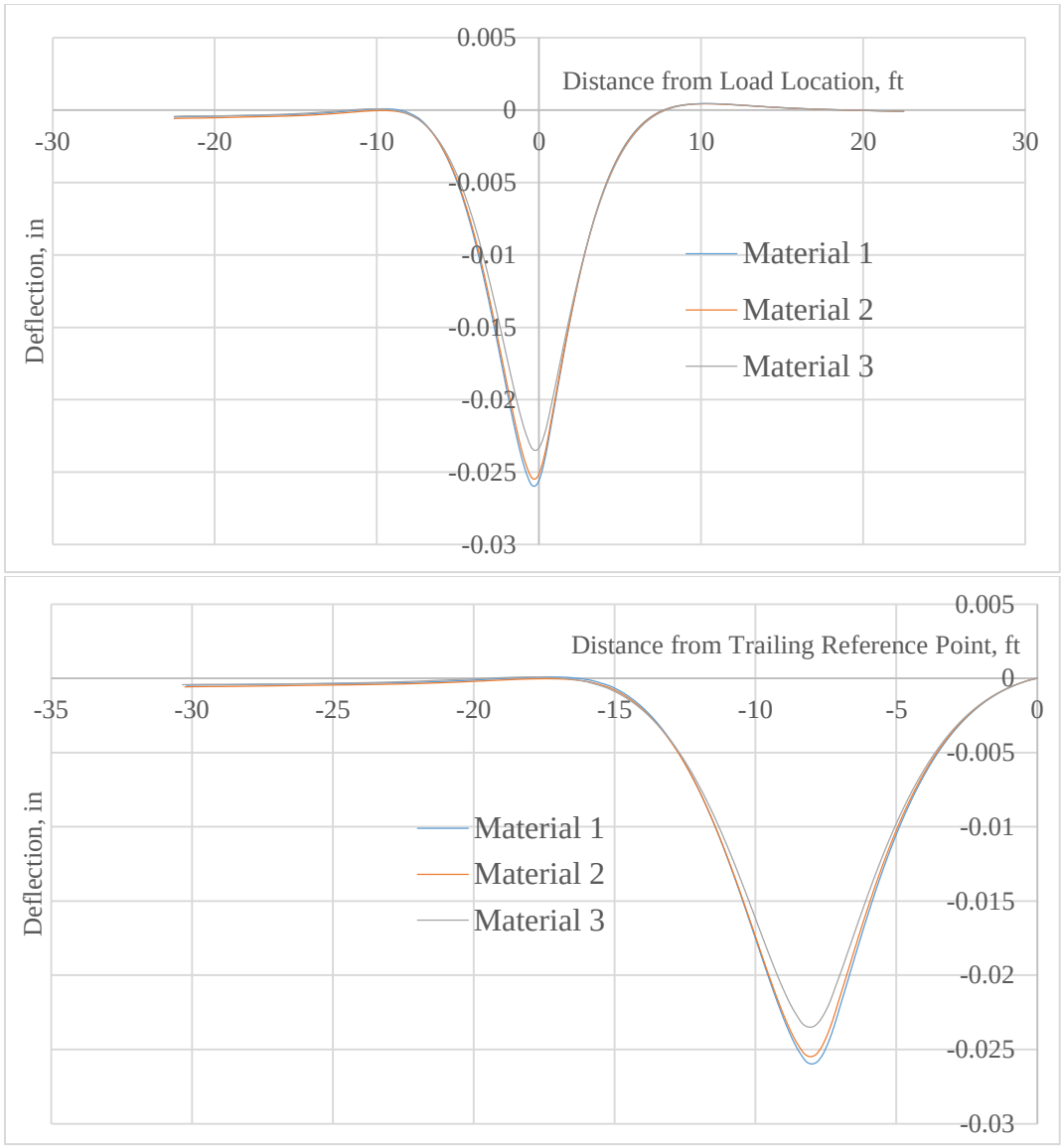

Figure B.3 (a)-(b) Pavements under Moving Loads v=40 mph Using 'Visco' Analysis

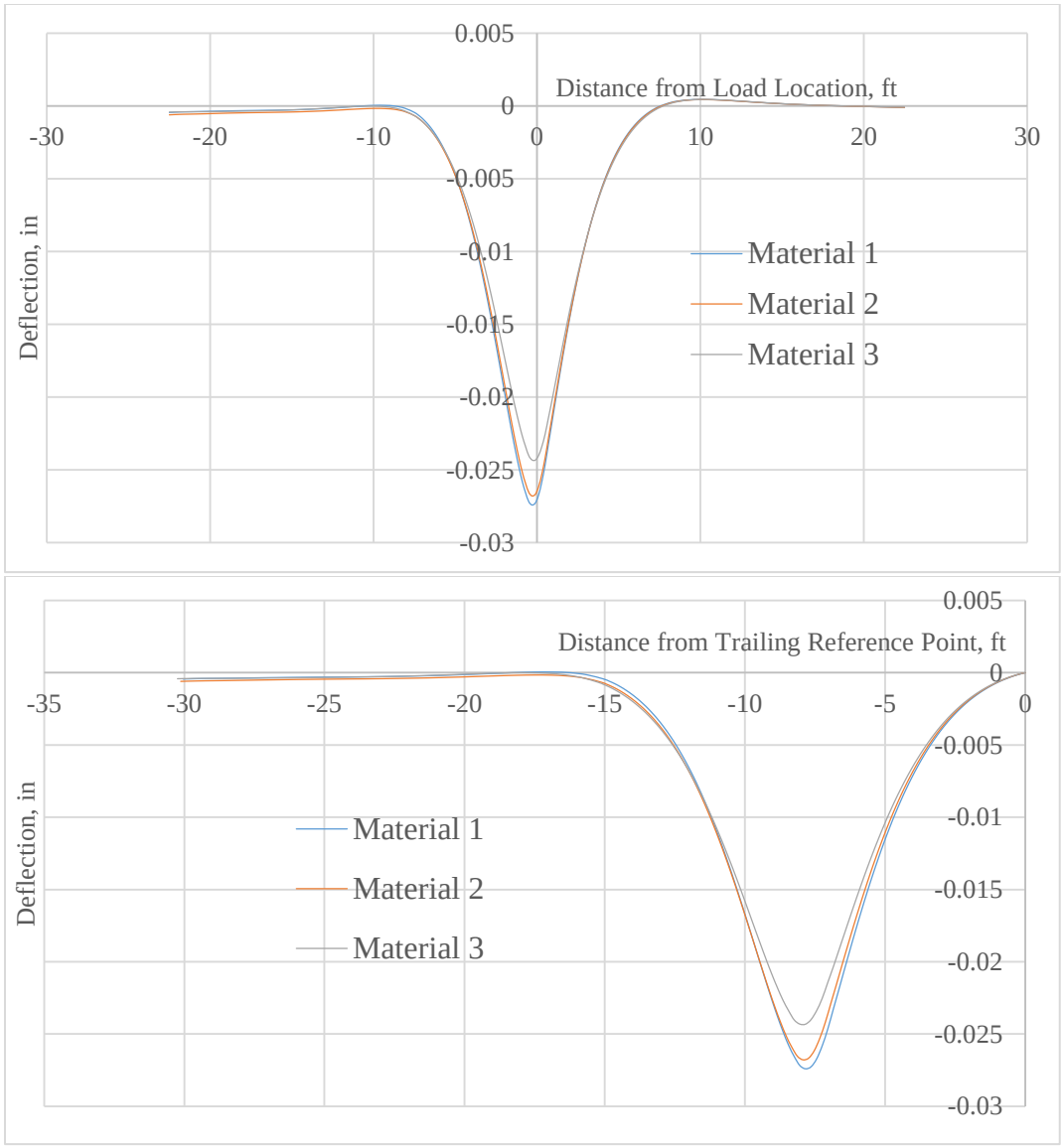

Figure B.4 (a)-(b) Pavements under Moving Loads v=25 mph Using 'Visco' Analysis

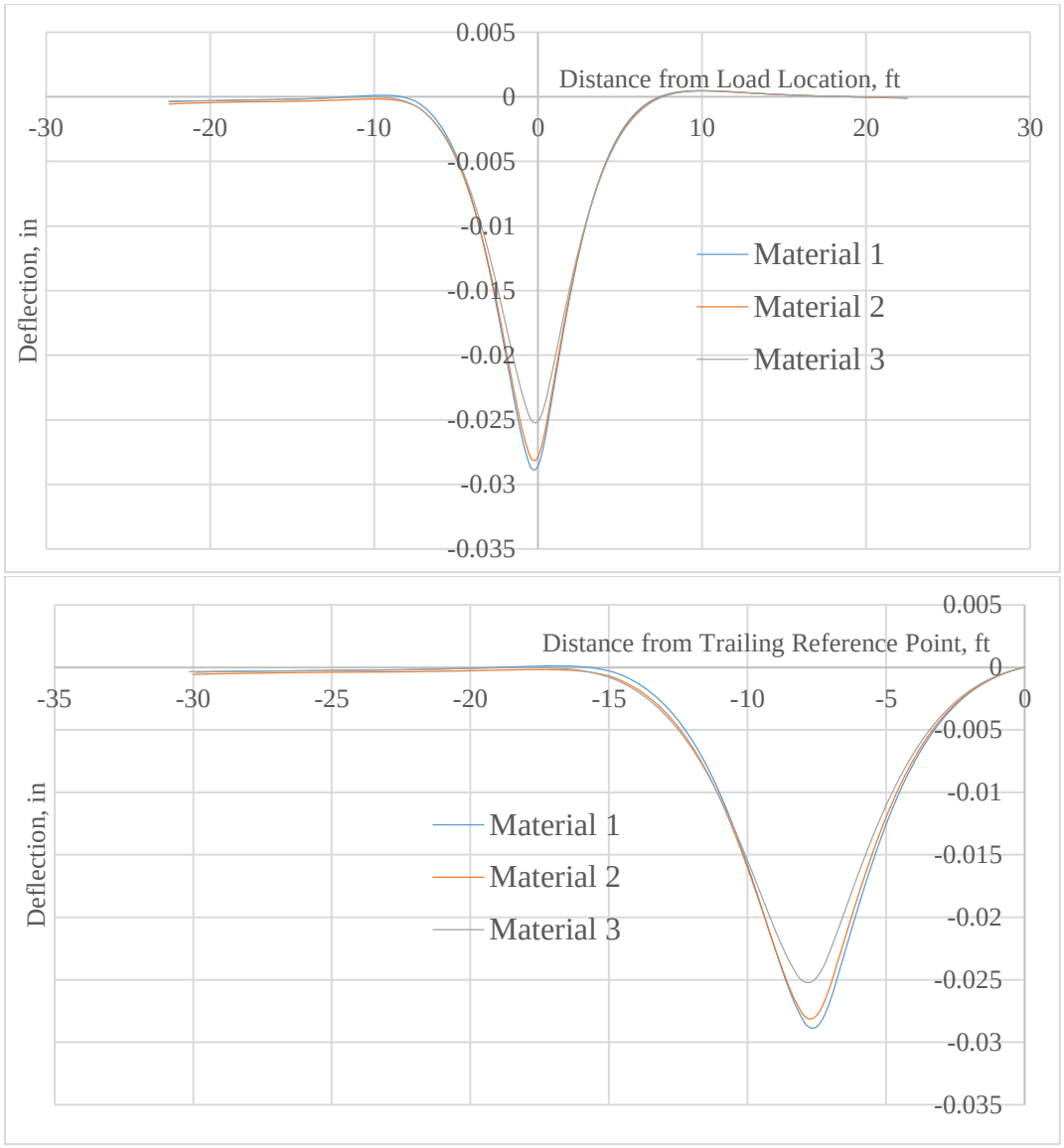

Figure B.5 (a)-(b) Pavements under Moving Loads v=15 mph Using 'Visco' Analysis

APPENDIX C

DEFLECTION BASINS OF 'DYNAMIC' ANALYSIS

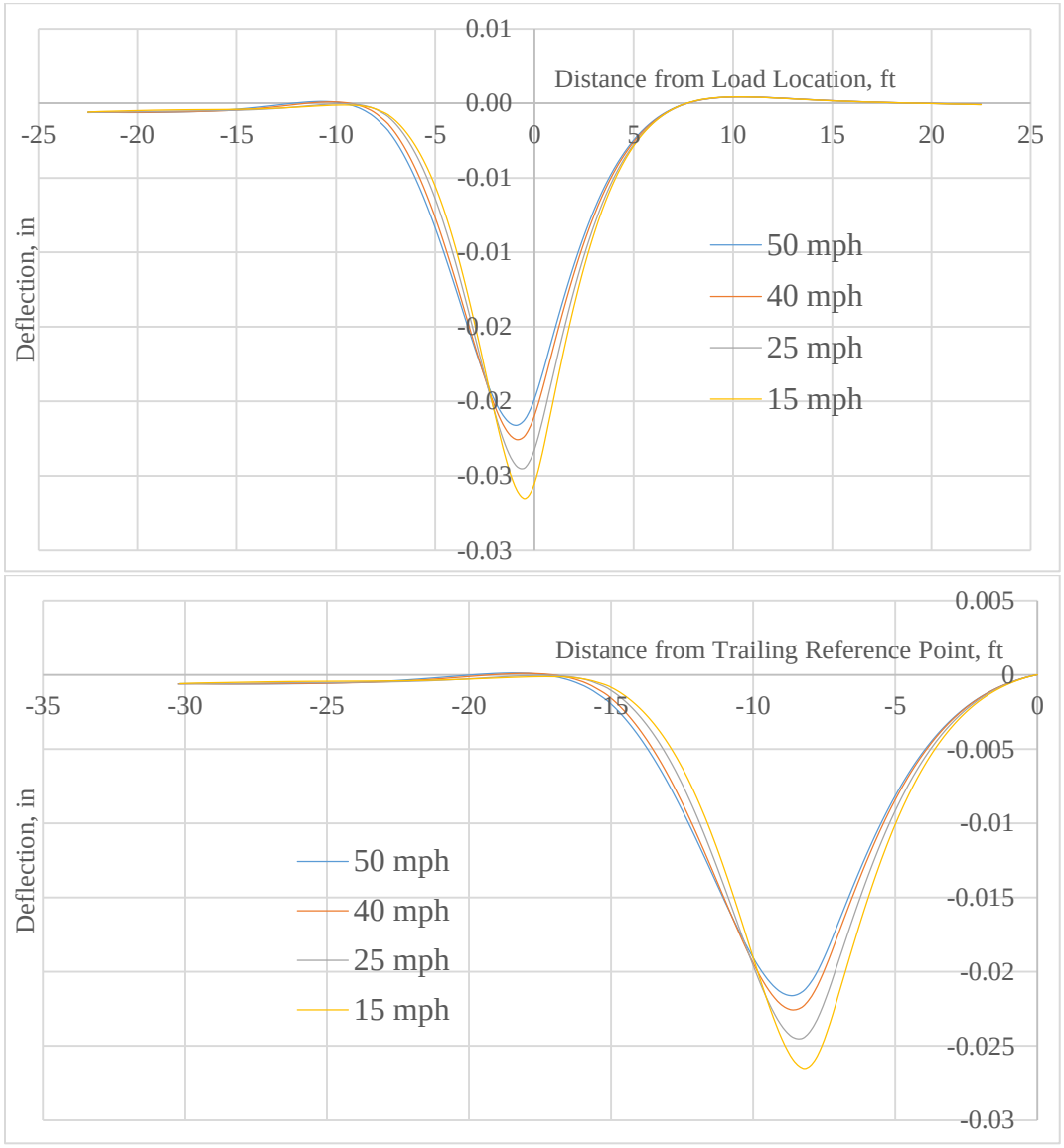

Figure C.1 (a)-(b) Pavement Type 2 under Different Moving Loads Using 'Dynamic' Analysis

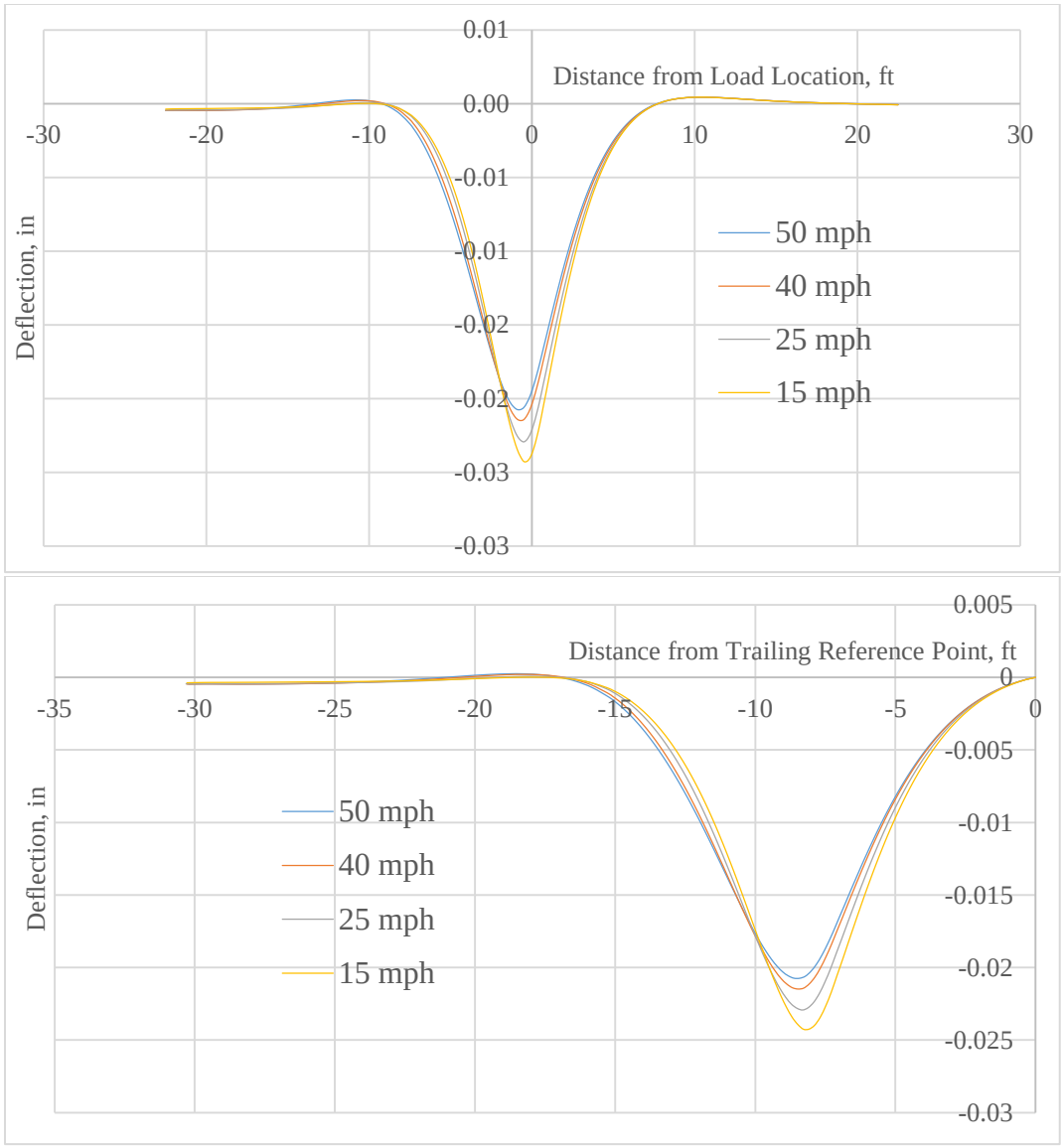

Figure C.2 (a)-(b) Pavement Type 3 under Different Moving Loads Using 'Dynamic' Analysis

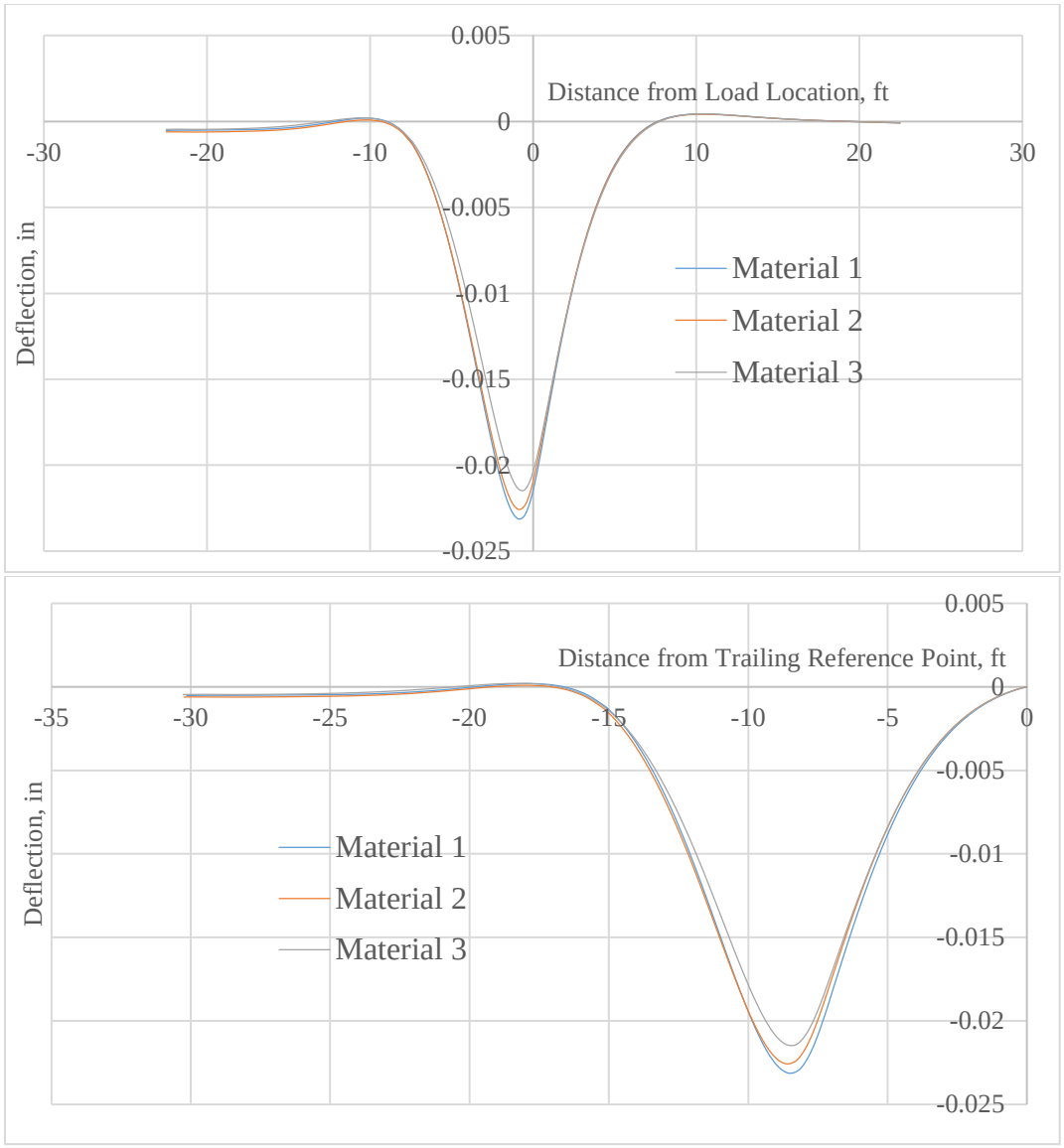

Figure C.3 (a)-(b) Pavements under Moving Loads v=40 mph Using ‘Dynamic’ Analysis

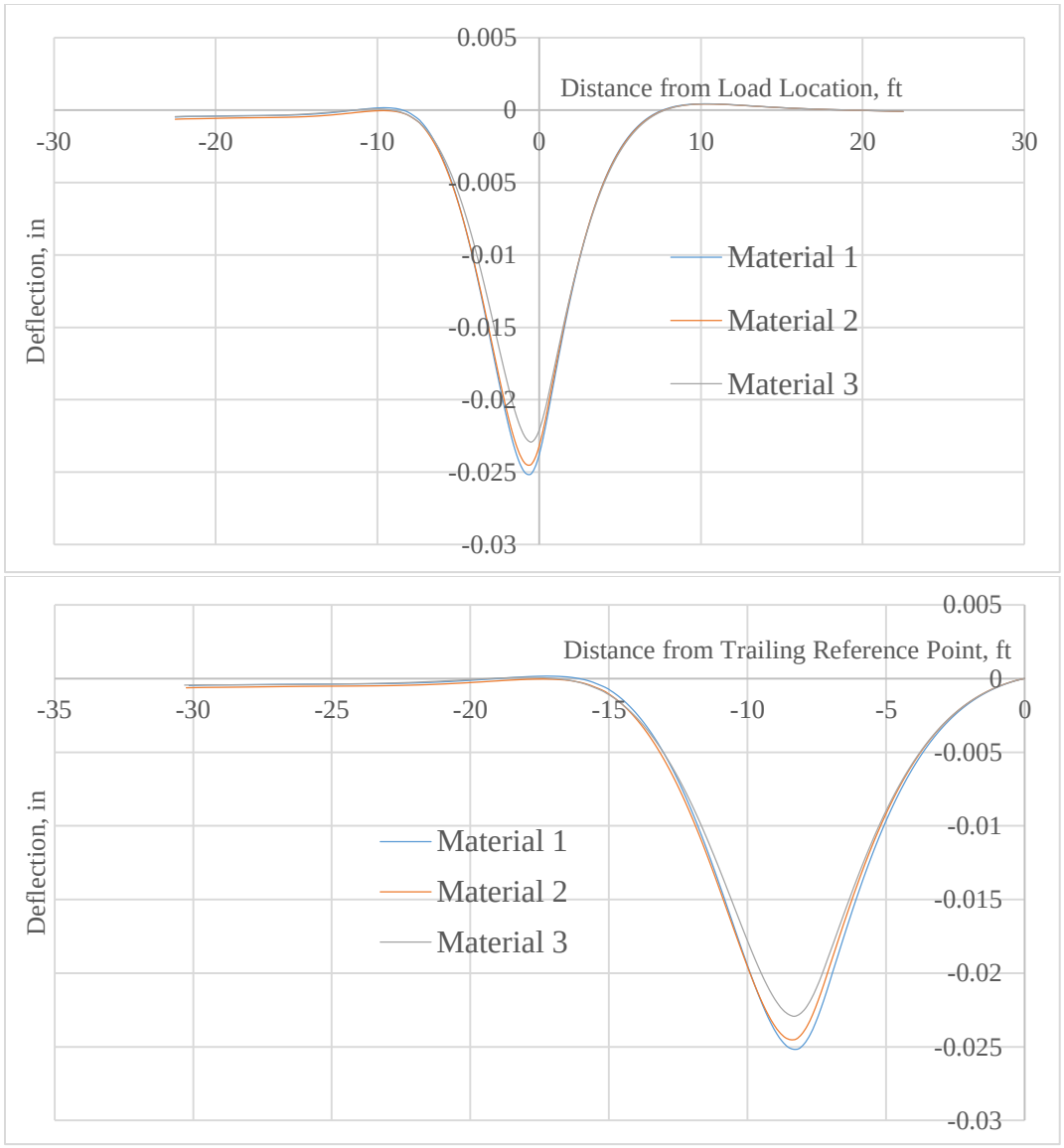

Figure C.4 (a)-(b) Pavements under Moving Loads v=25 mph Using ‘Dynamic’ Analysis

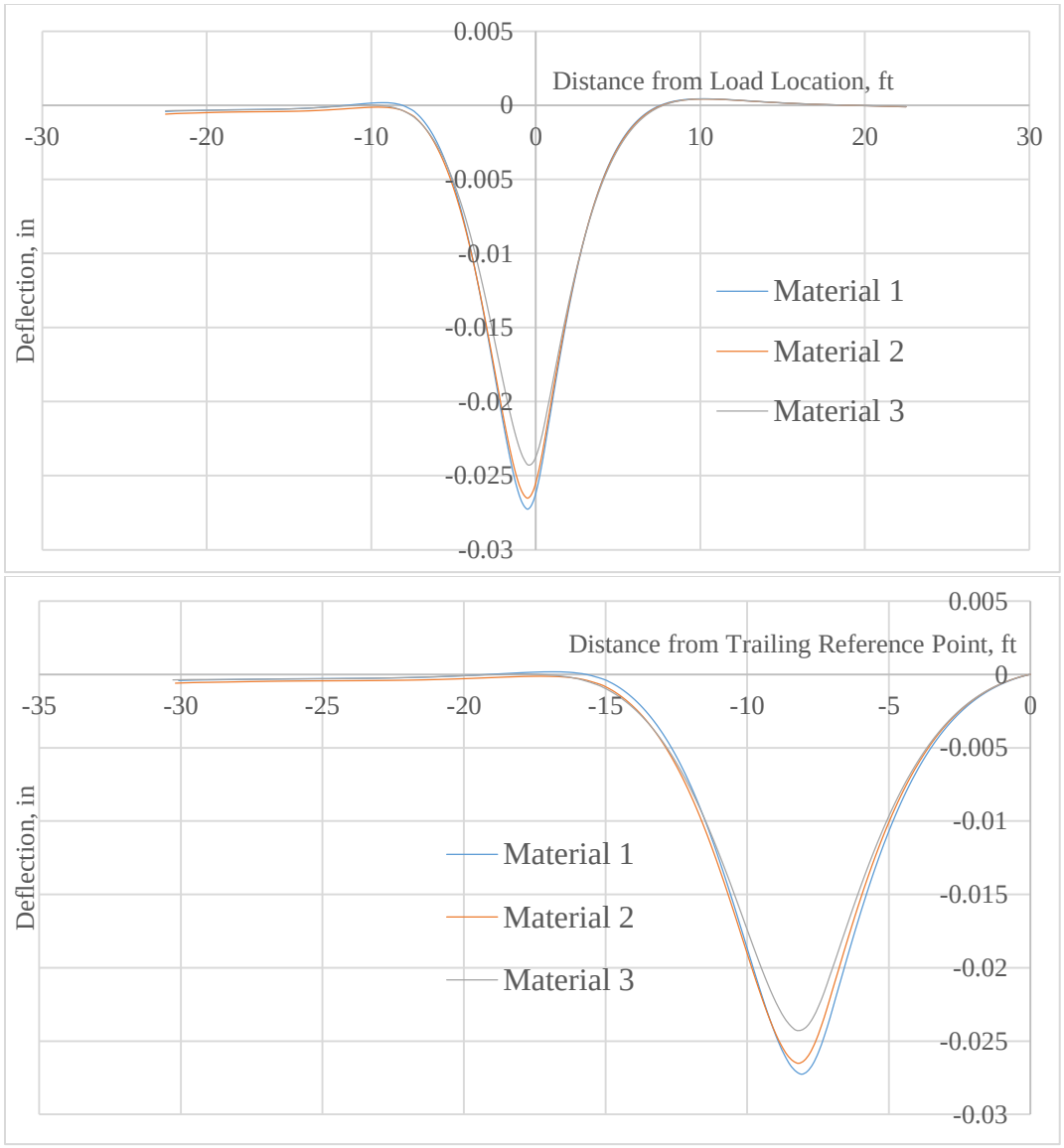

Figure C.5 (a)-(b) Pavements under Moving Loads v=15 mph Using ‘Dynamic’ Analysis